

# The Sivers Asymmetry in Hadronic Dijet Production

Zhong-Bo Kang,<sup>1,2,3,\*</sup> Kyle Lee,<sup>4,5,†</sup> Ding Yu Shao,<sup>1,2,3,‡</sup> and John Terry<sup>1,2,§</sup>

<sup>1</sup>*Department of Physics and Astronomy, University of California, Los Angeles, California 90095, USA*

<sup>2</sup>*Mani L. Bhaumik Institute for Theoretical Physics,*

*University of California, Los Angeles, California 90095, USA*

<sup>3</sup>*Center for Frontiers in Nuclear Science, Stony Brook University, Stony Brook, New York 11794, USA*

<sup>4</sup>*C.N. Yang Institute for Theoretical Physics, Stony Brook University, Stony Brook, New York 11794, USA*

<sup>5</sup>*Department of Physics and Astronomy, Stony Brook University, Stony Brook, New York 11794, USA*

We study the single spin asymmetry in the back-to-back dijet production in transversely polarized proton-proton collisions. Such an asymmetry is generated by the Sivers functions in the incoming polarized proton. We propose a QCD formalism in terms of the transverse momentum dependent parton distribution functions, which allow us to resum the large logarithms that arise in the perturbative calculations. We make predictions for the Sivers asymmetry of hadronic dijet production at the kinematic region that is relevant to the experiment at the Relativistic Heavy Ion Collider (RHIC). We further compute the spin asymmetries in the selected positive and negative jet charge bins, to separate the contributions from  $u$ - and  $d$ -quark Sivers functions. We find that both the sign and size of our numerical results are roughly consistent with the preliminary results from the STAR collaboration at the RHIC.

## I. INTRODUCTION

Exploring transverse momentum dependent parton distribution functions (TMD PDFs) has become one of the major research topics in hadron physics in recent years [1]. TMD PDFs provide three-dimensional (3D) imaging of the nucleon in both the longitudinal and transverse momentum space, which is one of the scientific pillars at the future Electron-Ion Collider [2]. Such 3D imaging of the nucleon offers novel insights into the highly nontrivial non-perturbative QCD dynamics and correlations [3].

Sivers function is one of the most studied TMD PDFs in the community. It describes the distribution of unpolarized partons inside a transversely polarized nucleon, through a correlation between the transverse spin of the nucleon and the transverse momentum of the parton with respect to the nucleon's moving direction. The Sivers function was first introduced by Sivers in 1990s [4, 5] to describe the large single transverse spin asymmetries observed in single inclusive particle production in hadronic collisions, see e.g. [6, 7]. Since then, large single spin asymmetries have also been consistently observed in proton-proton collisions in high energy experiments at the Relativistic Heavy Ion Collider (RHIC) [8–13]. On the theoretical side, understanding the precise origin of such large spin asymmetries has triggered a lot of research in the QCD community [14–22]. The difficulty in understanding such asymmetries for single hadron production (such as pions) in proton-proton collisions lies in the fact that they could receive contributions from many different correlations. Beside Sivers type correlations whose collinear version is referred to as the Qiu-Sterman function [15, 23] in the incoming nucleon, there could also be similar correlations in the hadronization process when the parton fragments into the hadrons [17, 19, 21, 22, 24]. See [25] for a recent development along this direction.

Simultaneously Sivers asymmetry has also been studied in semi-inclusive deep inelastic scattering (SIDIS) by HERMES collaboration at DESY [26, 27], COMPASS collaboration at CERN [28, 29], and Jefferson Lab [30]. Because of the semi-inclusive nature of the process, one can isolate the contribution from the Sivers function via different azimuthal angular modulations [31]. One of the remarkable and unique properties of the Sivers functions is its non-universality nature. For example, based on parity and time-reversal invariance of QCD, one can show that quark Sivers functions in SIDIS are opposite to those in the Drell-Yan process [32–34]. Such a sign change has been studied and confirmed experimentally [35–38], though additional work remains to be done to quantify the change in more details [39].

Sivers effect has been continuously studied in proton-proton collisions at the RHIC. In order to eliminate the contributions from the spin correlations in the fragmentation process, utilizing jet production to study Sivers asymmetry has been explored in the experiment [13, 40, 41]. In particular, back-to-back dijet production in transversely polarized proton-proton collisions was proposed by Boer and Vogelsang in 2003 as a unique opportunity at the RHIC [42].

\* [zkang@physics.ucla.edu](mailto:zkang@physics.ucla.edu)

† [kunsu.lee@stonybrook.edu](mailto:kunsu.lee@stonybrook.edu)

‡ [dingyu.shao@cern.ch](mailto:dingyu.shao@cern.ch)

§ [johndterry@physics.ucla.edu](mailto:johndterry@physics.ucla.edu)

Active investigation has been performed both experimentally [41] and theoretically [43–45]. On the experimental side, the Siverson spin asymmetry for dijet production was found to be quite small, largely due to the cancellation between  $u$ - and  $d$ -quark Siverson functions, which have similar size but opposite sign [25, 46, 47]. On the theoretical side, dijet production in proton-proton collisions is also subject to TMD factorization breaking [48, 49]. These have slowed down the efforts in the detailed study of the Siverson effect in the dijet production.

Recently, there has been renewed interest in both experimental and theoretical sides along this direction. Experimentally, the STAR collaboration at the RHIC is analyzing the new data for dijet Siverson asymmetry, and is exploring a novel method based on a charge weighting method in separating the contributions from individual  $u$  and  $d$  quark Siverson functions [50]. The PHENIX collaboration at the RHIC is exploring the TMD factorization breaking effects via back-to-back dihadron and photon-hadron production in proton-proton collisions [51, 52]. Theoretically, there have been efforts in performing QCD resummation for such processes in back-to-back dijet [53, 54] and vector boson-jet production [55–57]. At the same time, a theoretical framework has been developed to study spin asymmetries in specific jet charge bin [58], which would facilitate the analysis of the dijet spin asymmetries by the STAR collaboration. In light of all these activities, we set out to develop a resummation formalism for studying the Siverson asymmetry in back-to-back dijet production in transversely polarized proton-proton collisions. We make predictions for the dijet Siverson asymmetry in the kinematics relevant to the RHIC energy, to be compared with the experimental measurement in the near future.

The rest of the paper is organized as follows. In Section II, we summarized QCD formalism for dijet production in both unpolarized and polarized scatterings, and we provide a few remarks about our formalism. In Section III, we provide a procedure and demonstrate how to compute the process-dependent polarized hard functions in the color matrix form. In Section IV, we present the renormalization group evolution of all the relevant functions in our formalism, and we provide the final resummation formula. Section V is devoted to the phenomenological studies, where we make predictions for dijet Siverson asymmetry in the kinematic region relevant to the experiment at the RHIC. Since we are mainly interested in the Siverson asymmetry in the forward rapidity region where quark contributions dominate, we thus consider only the quark Siverson contribution and we neglect the gluon Siverson contribution. We summarize our paper in Section VI.

## II. QCD FORMALISM FOR DIJET PRODUCTION

In this paper, we study back-to-back dijet production in transversely polarized proton-proton collisions in the center-of mass frame,

$$p(P_A, \vec{S}_\perp) + p(P_B) \rightarrow J_1(y_c, \vec{P}_{1\perp}) + J_2(y_d, \vec{P}_{2\perp}) + X, \quad (1)$$

where the polarized proton with the momentum  $P_A$  and the transverse spin  $\vec{S}_\perp$  is moving in the  $+z$ -direction, while the unpolarized proton with the momentum  $P_B$  is moving in the  $-z$ -direction, and we have the center-of-mass energy  $s = (P_A + P_B)^2$ . The produced two jets  $J_1$  and  $J_2$  have rapidities  $y_{c,d}$  and transverse momenta  $\vec{P}_{1\perp}$  and  $\vec{P}_{2\perp}$ , respectively. These jets will be reconstructed via a suitable jet algorithm [59] and in the rest of the paper, we consider both of them to be anti- $k_T$  jets with jet radii  $R$ . In order to access the transverse motion of the partons inside the protons, we concentrate in the back-to-back region where the transverse momentum imbalance  $q_\perp$  is small. Here we define the average transverse momentum  $P_\perp$  of the two jets and the transverse momentum imbalance  $\vec{q}_\perp$  as follows

$$P_\perp = |\vec{P}_{1\perp} - \vec{P}_{2\perp}|/2, \quad \vec{q}_\perp = \vec{P}_{1\perp} + \vec{P}_{2\perp}, \quad (2)$$

where one has  $q_\perp \ll P_\perp$  in the back-to-back region. The production of such back-to-back dijets is illustrated in Fig. 1. In the transversely polarized proton-proton collisions, the transverse spin vector  $\vec{S}_\perp$  of the incoming proton and the transverse momentum imbalance  $\vec{q}_\perp$  of the two jets will be correlated, as advocated in [42]. Such a correlation leads to a  $\sin(\phi_q - \phi_S)$ -azimuthal modulation in the cross section with  $\phi_q$  and  $\phi_S$  the azimuthal angles of  $\vec{q}_\perp$  and  $\vec{S}_\perp$ , which arises precisely from the Siverson function in the polarized proton. Below we summarize the factorized formalism for dijet production in both unpolarized and polarized proton-proton collisions, and we provide more details for the relevant ingredients in the next section.

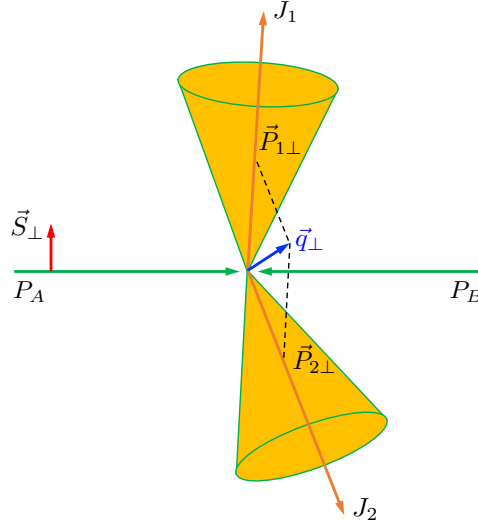


FIG. 1. Illustration of back-to-back dijet production in transversely polarized proton-proton collisions:  $p(P_A, \vec{S}_\perp) + p(P_B) \rightarrow J_1(y_c, \vec{P}_{1\perp}) + J_2(y_d, \vec{P}_{2\perp}) + X$ . The polarized proton with momentum  $P_A$  and transverse spin  $\vec{S}_\perp$  is moving in  $+z$ -direction, while the unpolarized proton with momentum  $P_B$  is moving in  $-z$ -direction. We have jet rapidities  $y_{c,d}$  and transverse momenta  $\vec{P}_{1\perp}$  and  $\vec{P}_{2\perp}$ , respectively. The dijet transverse momentum imbalance is defined as  $\vec{q}_\perp = \vec{P}_{1\perp} + \vec{P}_{2\perp}$ . Siverts asymmetry is generated due to the correlation between  $\vec{S}_\perp$  and  $\vec{q}_\perp$ .

### A. Dijet unpolarized cross section

In the back-to-back region where  $q_\perp \ll P_\perp$ , within the framework of soft-collinear effective theory (SCET) [60–64], one can write down a factorized form for the unpolarized differential cross section

$$\frac{d\sigma}{dy_c dy_d dP_\perp^2 d^2\vec{q}_\perp} = \sum_{abcd} \frac{1}{16\pi^2 \hat{s}^2} \frac{1}{N_{\text{init}}} \frac{1}{1 + \delta_{cd}} \int_{\perp} x_a f_a^{\text{unsub}}(x_a, k_{a\perp}, \mu, \nu) x_b f_b^{\text{unsub}}(x_b, k_{b\perp}, \mu, \nu) \times \text{Tr}[\mathbf{S}_{ab \rightarrow cd}(\lambda_\perp, \mu, \nu) \cdot \mathbf{H}_{ab \rightarrow cd}(P_\perp, \mu)] J_c(P_\perp R, \mu) S_c^{\text{CS}}(k_{c\perp}, R, \mu) J_d(P_\perp R, \mu) S_d^{\text{CS}}(k_{d\perp}, R, \mu), \quad (3)$$

where  $\hat{s} = x_a x_b s$  is the partonic center-of-mass energy,  $N_{\text{init}}$  is the corresponding spin- and color-averaged factor for each channel, while  $1/(1 + \delta_{cd})$  arises from the symmetry factor due to identical partons in the final state. We have used the following short-hand notation

$$\int_{\perp} = \int d^2\vec{k}_{a\perp} d^2\vec{k}_{b\perp} d^2\vec{k}_{c\perp} d^2\vec{k}_{d\perp} d^2\vec{\lambda}_\perp \delta^{(2)}(\vec{k}_{a\perp} + \vec{k}_{b\perp} + \vec{k}_{c\perp} + \vec{k}_{d\perp} + \vec{\lambda}_\perp - \vec{q}_\perp). \quad (4)$$

In Eq. (3),  $f_a^{\text{unsub}}(x_a, k_{a\perp}, \mu, \nu)$  and  $f_b^{\text{unsub}}(x_b, k_{b\perp}, \mu, \nu)$  are the so-called unsubtracted TMD PDFs, which carry the longitudinal momentum fractions  $x_{a,b}$  of the proton and the transverse momenta  $k_{a\perp}$  and  $k_{b\perp}$  with respect to their corresponding proton, and we have

$$x_a = \frac{P_\perp}{\sqrt{s}} (e^{y_c} + e^{y_d}), \quad x_b = \frac{P_\perp}{\sqrt{s}} (e^{-y_c} + e^{-y_d}), \quad (5)$$

where  $y_c, y_d$  are the rapidities of the two leading jets.

After performing Fourier transform for Eq. (3), we obtain the factorized formula in the coordinate  $b$ -space as follows

$$\frac{d\sigma}{dy_c dy_d dP_\perp^2 d^2\vec{q}_\perp} = \sum_{abcd} \frac{1}{16\pi^2 \hat{s}^2} \frac{1}{N_{\text{init}}} \frac{1}{1 + \delta_{cd}} \int \frac{d^2\vec{b}}{(2\pi)^2} e^{i\vec{q}_\perp \cdot \vec{b}} x_a f_a^{\text{unsub}}(x_a, b, \mu, \nu) x_b f_b^{\text{unsub}}(x_b, b, \mu, \nu) \times \text{Tr}[\mathbf{S}_{ab \rightarrow cd}(b, \mu, \nu) \cdot \mathbf{H}_{ab \rightarrow cd}(P_\perp, \mu)] J_c(P_\perp R, \mu) S_c^{\text{CS}}(b, R, \mu) J_d(P_\perp R, \mu) S_d^{\text{CS}}(b, R, \mu), \quad (6)$$

where  $f_a^{\text{unsub}}(x_a, b, \mu, \nu)$  and  $f_b^{\text{unsub}}(x_b, b, \mu, \nu)$  are the Fourier transform of  $f_a^{\text{unsub}}(x_a, k_{a\perp}, \mu, \nu)$  and  $f_b^{\text{unsub}}(x_b, k_{b\perp}, \mu, \nu)$ , respectively. On the other hand,  $\mathbf{H}_{ab \rightarrow cd}(P_\perp, \mu)$  is the hard function, while  $\mathbf{S}_{ab \rightarrow cd}(b, \mu, \nu)$  is a global soft function.

Note that both the hard function  $\mathbf{H}_{ab \rightarrow cd}$  and the global soft function  $\mathbf{S}_{ab \rightarrow cd}$  are expressed in the matrix form in the color space and the trace  $\text{Tr}[\dots]$  is over the color. Such factorization of the hard and soft function into matrix form is essential to capture evolution effects between the hard scale  $\sim P_\perp$  and the imbalance scale  $\sim q_\perp$  [65]. Here  $\mu$  and  $\nu$  denotes renormalization and rapidity scales, separately. The rapidity scale  $\nu$  arises because both the TMD PDFs and the global soft functions have rapidity divergence [66, 67], which are canceled between them as demonstrated below. This cancellation allows us to define rapidity divergence independent  $\tilde{\mathbf{S}}_{ab \rightarrow cd}(b, \mu)$  by

$$\mathbf{S}_{ab \rightarrow cd}(b, \mu, \nu) = \tilde{\mathbf{S}}_{ab \rightarrow cd}(b, \mu) S_{ab}(b, \mu, \nu), \quad (7)$$

where  $S_{ab}(b, \mu, \nu)$  is the standard soft function appearing in usual Drell-Yan and SIDIS processes. This explicit redefinition allows us to subtract the rapidity divergence from the unsubtracted TMD PDFs to define the standard TMD PDFs  $f_i(x_i, b, \mu)$  that are free of rapidity divergence as [68]

$$f_a^{\text{unsub}}(x_a, b, \mu, \nu) f_b^{\text{unsub}}(x_b, b, \mu, \nu) S_{ab}(b, \mu, \nu) \rightarrow f_a(x_a, b, \mu) f_b(x_b, b, \mu). \quad (8)$$

Note that the properly-defined TMD PDFs  $f_a(x_a, b, \mu)$  and  $f_b(x_b, b, \mu)$  are no long subject to the rapidity divergence and this is why there are no explicit  $\nu$ -dependence in the arguments any more. Such defined unpolarized TMD PDFs are the same as those probed in the standard SIDIS and Drell-Yan processes.

The jet functions  $J_c(P_\perp R, \mu)$  and  $J_d(P_\perp R, \mu)$  in Eq. (6) describe the creation of anti- $k_T$  jets from the partons  $c$  and  $d$ , respectively. Finally,  $S_c^{\text{cs}}(k_{c\perp}, R, \mu)$  and  $S_d^{\text{cs}}(k_{d\perp}, R, \mu)$  are the collinear-soft functions. They describe soft gluon radiation with separations of order  $R$  along the jet direction, which can resolve the substructure of the jet. If one performs the integration over the azimuthal angle of the vector  $\vec{b}$ , we obtain the following expression

$$\begin{aligned} \frac{d\sigma}{dy_c dy_d dP_\perp^2 d^2\vec{q}_\perp} &= \sum_{abcd} \frac{1}{16\pi^2 \hat{s}^2} \frac{1}{N_{\text{init}}} \frac{1}{1 + \delta_{cd}} \frac{1}{2\pi} \int_0^\infty db b J_0(q_\perp b) x_a f_a(x_a, b, \mu) x_b f_b(x_b, b, \mu) \\ &\times \text{Tr} \left[ \tilde{\mathbf{S}}_{ab \rightarrow cd}(b, \mu) \cdot \mathbf{H}_{ab \rightarrow cd}(P_\perp, \mu) \right] J_c(P_\perp R, \mu) S_c^{\text{cs}}(b, R, \mu) J_d(P_\perp R, \mu) S_d^{\text{cs}}(b, R, \mu), \end{aligned} \quad (9)$$

where  $J_0$  is the Bessel function of order zero.

## B. Dijet Siverson asymmetry

In the transversely polarized proton-proton collisions, the Siverson function will lead to a spin asymmetry in the cross section when one flips the transverse spin of the incoming proton. We thus define the difference in the cross section as  $d\Delta\sigma(S_\perp) = [d\sigma(S_\perp) - d\sigma(-S_\perp)]/2$ . One can write down a similar factorized formula for such a spin-dependent differential cross section following Eq. (3), and it is given by

$$\begin{aligned} \frac{d\Delta\sigma(S_\perp)}{dy_c dy_d dP_\perp^2 d^2\vec{q}_\perp} &= \sum_{abcd} \frac{1}{16\pi^2 \hat{s}^2} \frac{1}{N_{\text{init}}} \frac{1}{1 + \delta_{cd}} \int_\perp \frac{1}{M} \epsilon_{\alpha\beta} S_\perp^\alpha k_{a\perp}^\beta x_a f_{1T}^{\perp a, \text{unsub}}(x_a, k_{a\perp}, \mu, \nu) x_b f_b^{\text{unsub}}(x_b, k_{a\perp}, \mu, \nu) \\ &\times \text{Tr} \left[ \mathbf{S}_{ab \rightarrow cd}(\lambda_\perp, \mu, \nu) \cdot \mathbf{H}_{ab \rightarrow cd}^{\text{Siverson}}(P_\perp, \mu) \right] J_c(P_\perp R, \mu) S_c^{\text{cs}}(k_{c\perp}, R, \mu) J_d(P_\perp R, \mu) S_d^{\text{cs}}(k_{d\perp}, R, \mu), \end{aligned} \quad (10)$$

where  $\epsilon_{\alpha\beta}$  is a two-dimensional asymmetric tensor with  $\epsilon_{12} = +1$ , and we have replaced the unpolarized TMD PDF in Eq. (3) by the Siverson function in the above equation following the so-called Trento convention [69],

$$f_a^{\text{unsub}}(x_a, k_{a\perp}, \mu, \nu) \rightarrow \frac{1}{M} \epsilon_{\alpha\beta} S_\perp^\alpha k_{a\perp}^\beta f_{1T}^{\perp a, \text{unsub}}(x_a, k_{a\perp}, \mu, \nu). \quad (11)$$

Note that we have also assumed that the global soft function  $\mathbf{S}_{ab \rightarrow cd}(\lambda_\perp, \mu, \nu)$  stays the same as that of the unpolarized collisions in Eq. (3). Although this is a reasonable assumption since the soft gluon radiation should be spin-independent, this has to be carefully checked and we leave this for future investigation.

Performing Fourier transform from the transverse momentum space into the  $b$ -space, we obtain

$$\begin{aligned} \frac{d\Delta\sigma(S_\perp)}{dy_c dy_d dP_\perp^2 d^2\vec{q}_\perp} &= \sum_{abcd} \frac{1}{16\pi^2 \hat{s}^2} \frac{1}{N_{\text{init}}} \frac{1}{1 + \delta_{cd}} \epsilon_{\alpha\beta} S_\perp^\alpha \int \frac{d^2\vec{b}}{(2\pi)^2} e^{i\vec{q}_\perp \cdot \vec{b}} x_a f_{1T}^{\perp a(\beta)}(x_a, b, \mu) x_b f_b(x_b, b, \mu) \\ &\times \text{Tr} \left[ \tilde{\mathbf{S}}_{ab \rightarrow cd}(b, \mu) \cdot \mathbf{H}_{ab \rightarrow cd}^{\text{Siverson}}(P_\perp, \mu) \right] J_c(P_\perp R, \mu) S_c^{\text{cs}}(b, R, \mu) J_d(P_\perp R, \mu) S_d^{\text{cs}}(b, R, \mu), \end{aligned} \quad (12)$$

where we have already used Eq. (7) to rewrite the unsubtracted unpolarized TMD PDF and Siverson function in terms of the properly defined versions which are free of rapidity divergence. Here  $f_{1T}^{\perp a(\beta)}(x_a, b, \mu)$  is the Fourier transform of the Siverson function,

$$\begin{aligned} f_{1T}^{\perp a(\beta)}(x_a, b, \mu) &= \frac{1}{M} \int d^2 \vec{k}_{a\perp} e^{-i \vec{k}_{a\perp} \cdot \vec{b}} k_{a\perp}^\beta f_{1T}^{\perp a}(x_a, k_{a\perp}, \mu), \\ &\equiv \left( \frac{ib^\beta}{2} \right) \hat{f}_{1T}^{\perp a}(x_a, b, \mu), \end{aligned} \quad (13)$$

where we have used the fact that the integration in the first line would be proportional to  $b^\beta$ , and we thus factored  $b^\beta$  out explicitly in the second line<sup>1</sup>. The remaining part of the Siverson function is now denoted as  $\hat{f}_{1T}^{\perp a}(x_a, b, \mu)$ . Note that for the same reason as explained below Eq. (8), we do not have the rapidity  $\nu$ -dependence in the above equation. It is also instructive to emphasize that  $\hat{f}_{1T}^{\perp a}(x_a, b, \mu)$  follows the same TMD evolution equations as the unpolarized TMD PDF  $f_a(x_a, b, \mu)$ , which enables us to evolve the Siverson function from some initial scale  $\mu_0$  to the relevant scale  $\mu$ . On the other hand, at the initial scale  $\mu_0$ , the Siverson function  $\hat{f}_{1T}^{\perp a}(x_a, b, \mu)$  can be further matched onto the collinear twist-3 Qiu-Sterman function  $T_{a,F}(x_1, x_2, \mu)$ . For example, at a specific scale  $\mu_b = b_0/b$  with  $b_0 = 2e^{-\gamma_E}$ , one has the following expression for quark Siverson functions

$$\hat{f}_{1T}^{\perp q}(x_a, b, \mu_b) = \int_{x_a}^1 \frac{dx}{x} C_{q \leftarrow q'} \left( \frac{x_a}{x}, \mu_b \right) T_{q',F}(x, x, \mu_b), \quad (14)$$

where the matching coefficients at the NLO are given by [70–74]

$$C_{q \leftarrow q'}(x, \mu_b) = \delta_{qq'} \left[ \delta(1-x) + \frac{\alpha_s(\mu_b)}{2\pi} \left( -\frac{1}{2N_c} \right) (1-x) \right]. \quad (15)$$

We now plug Eq. (13) into Eq. (12), and integrate over the azimuthal angle of the vector  $\vec{b}$ , we obtain

$$\begin{aligned} \frac{d\Delta\sigma(S_\perp)}{dy_c dy_d dP_\perp^2 d^2 \vec{q}_\perp} &= \sin(\phi_q - \phi_S) \sum_{abcd} \frac{1}{16\pi^2 \hat{s}^2} \frac{1}{N_{\text{init}}} \frac{1}{1 + \delta_{cd}} \left( -\frac{1}{4\pi} \right) \int_0^\infty db b^2 J_1(q_\perp b) x_a \hat{f}_{1T}^{\perp a}(x_a, b, \mu) x_b f_b(x_b, b, \mu) \\ &\times \text{Tr} \left[ \tilde{\mathbf{S}}_{ab \rightarrow cd}(b, \mu) \cdot \mathbf{H}_{ab \rightarrow cd}^{\text{Sivers}}(P_\perp, \mu) \right] J_c(P_\perp R, \mu) S_c^{\text{CS}}(b, R, \mu) J_d(P_\perp R, \mu) S_d^{\text{CS}}(b, R, \mu), \end{aligned} \quad (16)$$

where  $J_1$  is the Bessel function of order one, and we have used the identity

$$\epsilon_{\alpha\beta} S_\perp^\alpha \hat{q}_\perp^\beta = \sin(\phi_q - \phi_S), \quad (17)$$

with  $\hat{q}_\perp$  the unit vector along the direction of the imbalance  $\vec{q}_\perp$ . In general, the so-called single spin asymmetry (the Siverson asymmetry)  $A_N$  for dijet production will be then given by

$$A_N = \frac{d\Delta\sigma(S_\perp)}{dy_c dy_d dP_\perp^2 d^2 \vec{q}_\perp} \bigg/ \frac{d\sigma}{dy_c dy_d dP_\perp^2 d^2 \vec{q}_\perp}. \quad (18)$$

Finally, since the Siverson function is not universal, one has to carefully include those non-universality or process-dependence into the above formalism [43–45, 68, 75–77]. We have chosen to include all such process-dependence into the hard function  $\mathbf{H}_{ab \rightarrow cd}^{\text{Sivers}}(P_\perp, \mu)$ , and this way the Siverson functions in Eq. (16) are the same as those probed in the SIDIS process. We explain in details how we derive the hard functions  $\mathbf{H}_{ab \rightarrow cd}^{\text{Sivers}}$  for different partonic processes in the next section.

### C. Remarks

We will provide detailed expressions and discuss the evolution of all the relevant functions in the next section. Here, let us emphasize the following points on our factorized formalism:

<sup>1</sup> To make the matching coefficient normalized to 1 at the lowest order in Eq. (14), we include the additional factor of  $i/2$  in Eq. (13).

- Eqs. (6) and (12) are our proposed factorized formulas for dijet production in unpolarized and transversely polarized proton-proton collisions, respectively. They are the essential theoretical formalism we are using in the phenomenology section to compute the dijet Sivvers asymmetry, which can be compared with the experimental data at the RHIC.
- It is important to emphasize that we have derived both Eqs. (6) and (12) within the SCET framework, in which the Glauber mode is absent. However, it is well-known that the inclusion of the Glauber modes will lead to factorization breaking. The factorization violation effects from Glauber gluon exchanging diagrams between two incoming nucleons have been discussed in [48, 49, 78, 79]. In principle, such effects can be systematically accounted for in SCET by including explicitly the Glauber mode [80]. How exactly this works for dijet production remains to be investigated. In any case, the formalism we presented here would be a good starting point. Not only this formalism incorporates the process dependence of the Sivvers functions as outlined in [43–45, 75, 77], but also it properly takes care of the QCD resummation and evolution effects and thus is able to study the energy and scale dependence of the Sivvers asymmetry as measured in the experiment.
- There will be non-global structures from quantum correlations between in-jet and out-of-jet radiations: exclusive jet production will be sensitive on the correlation effects between in-jet and out-of-jet radiations, which is first discovered in [81]. The corresponding factorization and resummation formula involves multi-Wilson-line structures [82, 83], which will give the non-linear evolution equation [84] for Non-Global Logarithms (NGLs) resummation. The TMD factorization formula including such effects have been given in [56, 85, 86]. Numerically, the leading-order NGLs resummation can be solved using parton shower methods [81, 87–89] or BMS equations [90, 91]. In our phenomenology, we have included the contributions from NGLs as discussed in Section V.
- Our formalism for unpolarized dijet production in Eqs. (6) is similar to those in [53, 54]. Here, by taking the small- $R$  limit, we refactorize the TMD  $R$ -dependence soft function [53, 54] as the product of the  $R$ -independent global TMD soft function and the  $R$ -dependent collinear-soft function [55, 56]. In addition, the  $R$ -dependent hard function in [53, 54] has been further factorized into a  $R$ -independent hard function as above and the jet functions which naturally capture all the  $R$ -dependence. In this regard, the factorized formula presented here is more transparent and intuitive. Such refactorizations are essential to resum logarithms of  $R$  for small radius jets.

### III. HARD FUNCTIONS IN UNPOLARIZED AND POLARIZED SCATTERING

In this section, we derive the hard functions for both unpolarized and polarized scatterings, i.e.  $\mathbf{H}_{ab \rightarrow cd}(P_\perp, \mu)$  and  $\mathbf{H}_{ab \rightarrow cd}^{\text{Sivvers}}(P_\perp, \mu)$  in Eqs. (9) and (16), respectively. They are matrices in the color space. We first review the results for the hard functions  $\mathbf{H}_{ab \rightarrow cd}$  in the unpolarized scattering, which are well-known in the literature, see e.g. Refs. [92, 93]. Using the notation developed, we then show how we derive the hard function matrices  $\mathbf{H}_{ab \rightarrow cd}^{\text{Sivvers}}$  in the polarized scattering case. These hard functions properly take into account the process-dependence of the Sivvers functions [43–45, 68, 75–77]. To get started, we define the Mandelstam variables for the partonic scattering process,  $a(p_1) + b(p_2) \rightarrow c(p_3) + d(p_4)$ , as follows

$$\hat{s} = (p_1 + p_2)^2 = (p_3 + p_4)^2 = 4P_\perp^2 \cosh^2\left(\frac{\Delta y}{2}\right) = x_a x_b s, \quad (19a)$$

$$\hat{t} = (p_1 - p_3)^2 = (p_2 - p_4)^2 = -2P_\perp^2 e^{-\Delta y/2} \cosh\left(\frac{\Delta y}{2}\right), \quad (19b)$$

$$\hat{u} = (p_1 - p_4)^2 = (p_2 - p_3)^2 = -2P_\perp^2 e^{\Delta y/2} \cosh\left(\frac{\Delta y}{2}\right), \quad (19c)$$

where  $\Delta y = y_c - y_d$  is the rapidity difference of the two jets. In the following, the expressions for the hard functions will be written in terms of these Mandelstam variables.

12 → 34	Color Basis	12 → 34	Color Basis	12 → 34	Color Basis
$qq' \rightarrow qq'$	$\Gamma_{31}\Gamma_{42}$	$q\bar{q} \rightarrow q'\bar{q}'$	$\Gamma_{21}\Gamma_{34}$	$q\bar{q}' \rightarrow \bar{q}'q$	$\Gamma_{41}\Gamma_{23}$
$qq' \rightarrow q'q$		$q\bar{q}' \rightarrow q\bar{q}'$		$q\bar{q} \rightarrow \bar{q}'q'$	
$qq' \rightarrow qq$		$q\bar{q} \rightarrow \bar{q}\bar{q}$		$q\bar{q} \rightarrow \bar{q}q$	
$\bar{q}\bar{q}' \rightarrow \bar{q}\bar{q}'$	$\Gamma_{13}\Gamma_{24}$	$\bar{q}\bar{q} \rightarrow \bar{q}'\bar{q}'$	$\Gamma_{12}\Gamma_{43}$	$\bar{q}\bar{q}' \rightarrow q'\bar{q}$	$\Gamma_{14}\Gamma_{32}$
$\bar{q}\bar{q}' \rightarrow \bar{q}'\bar{q}$		$\bar{q}\bar{q}' \rightarrow \bar{q}q'$		$\bar{q}q \rightarrow q'\bar{q}'$	
$\bar{q}\bar{q}' \rightarrow \bar{q}\bar{q}$		$\bar{q}q \rightarrow \bar{q}q$		$\bar{q}q \rightarrow q\bar{q}$	

TABLE I. The choice of basis for each of the four quark subprocesses.  $\Gamma_{ij}$  are operators in color space which join the fermion lines  $i$  and  $j$ .

## A. Unpolarized Hard Matrices

### 1. Four quark subprocesses

We start with the partonic subprocesses that involve four quarks, such as  $qq' \rightarrow qq'$ . An illustration of the factorization between the unpolarized TMD PDFs and the corresponding hard functions is given in Fig. 2. Here the lower blob represents the unpolarized quark TMD PDF,  $C^u$  is the color factor, and the additional factorization in the top side from the proton  $B$  is suppressed in the figure. In Tab. I, we organize each of the four quark subprocesses into a color basis. In this table,  $\Gamma_{ij}$  are operators in color space which act on particles  $i$  and  $j$ . The choice of these operators determines the color basis used to generate the hard and soft matrices. From this table, we see that there are in total 18 different color matrices which need to be computed. However, we note that the hard function for the unpolarized case is invariant under charge conjugation. So only the top row of each box must be calculated. Furthermore, once the hard matrices have been calculated for the first column, crossing symmetry can be applied in order to obtain the hard color matrices for the second and third column. It is then only necessary to calculate the hard matrices for the subprocesses associated with the color basis  $\Gamma_{31}\Gamma_{42}$ . For our calculation, we follow the conventions used in Refs. [92, 93] to choose  $\Gamma_{ij}^1 = (t^a)_{ij}$  and  $\Gamma_{ij}^2 = \delta_{ij}$ , so that the color basis is spanned by the operators

$$\theta_1 = (t^a)_{ij}(t^a)_{kl}, \quad \theta_2 = \delta_{ij}\delta_{kl}. \quad (20)$$

We note that other conventions have been used in the literature [94]. In order to compute the hard color matrices, we begin by decomposing the scattering amplitude of a process into the color space. For example, for the  $qq \rightarrow qq$  subprocess, we write

$$\mathcal{M} = \mathcal{M}_t + \mathcal{M}_u, \quad (21)$$

where we have suppressed the  $ab \rightarrow cd$  label and the subscript denotes the relevant Mandelstam variable ( $\hat{t}$  or  $\hat{u}$ ) for the channel that contributes to the subprocess. We can write these scattering amplitudes in color space as

$$\mathcal{M}_t = \mathcal{M}_{t1}\theta_1 + \mathcal{M}_{t2}\theta_2, \quad \mathcal{M}_u = \mathcal{M}_{u1}\theta_1 + \mathcal{M}_{u2}\theta_2. \quad (22)$$

Then we will have  $|\mathcal{M}|^2$  as

$$|\mathcal{M}|^2 = |\mathcal{M}_t|^2 + |\mathcal{M}_u|^2 + \mathcal{M}_t\mathcal{M}_u^\dagger + \mathcal{M}_u\mathcal{M}_t^\dagger, \quad (23)$$

where the individual terms can be written as follows

$$|\mathcal{M}_t|^2 = \text{Tr}[\mathbf{H}_{tt} \cdot \mathbf{S}], \quad |\mathcal{M}_u|^2 = \text{Tr}[\mathbf{H}_{uu} \cdot \mathbf{S}], \quad \mathcal{M}_u\mathcal{M}_t^\dagger = \text{Tr}[\mathbf{H}_{ut} \cdot \mathbf{S}], \quad \mathcal{M}_t\mathcal{M}_u^\dagger = \text{Tr}[\mathbf{H}_{tu} \cdot \mathbf{S}]. \quad (24)$$

Here we define the hard matrices in color space as

$$\mathbf{H}_{tt} = \begin{bmatrix} |\mathcal{M}_{t1}|^2 & \mathcal{M}_{t1}\mathcal{M}_{t2}^\dagger \\ \mathcal{M}_{t2}\mathcal{M}_{t1}^\dagger & |\mathcal{M}_{t2}|^2 \end{bmatrix}, \quad \mathbf{H}_{uu} = \begin{bmatrix} |\mathcal{M}_{u1}|^2 & \mathcal{M}_{u1}\mathcal{M}_{u2}^\dagger \\ \mathcal{M}_{u2}\mathcal{M}_{u1}^\dagger & |\mathcal{M}_{u2}|^2 \end{bmatrix}, \quad (25)$$

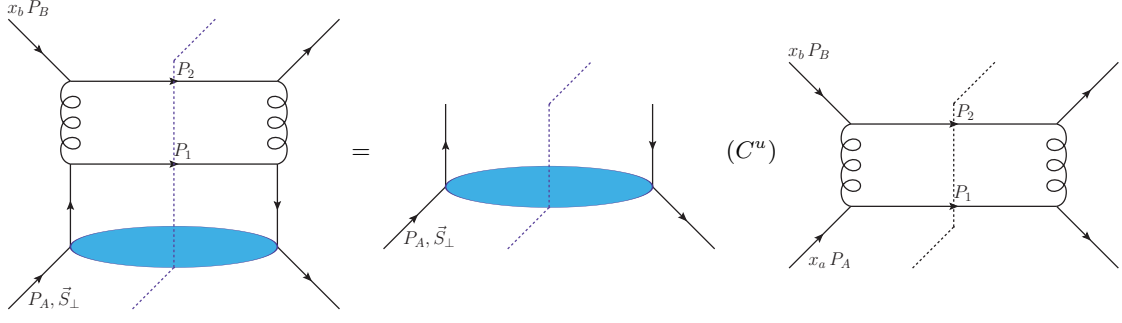


FIG. 2. A demonstration of the factorization for the unpolarized  $qq' \rightarrow qq'$  interaction. The color factors  $C_u$  contains the information on the color flow while the hard function is independent of this color.

$$\mathbf{H}_{ut} = \begin{bmatrix} \mathcal{M}_{u1} \mathcal{M}_{t1}^\dagger & \mathcal{M}_{u1} \mathcal{M}_{t2}^\dagger \\ \mathcal{M}_{u2} \mathcal{M}_{t1}^\dagger & \mathcal{M}_{u2} \mathcal{M}_{t2}^\dagger \end{bmatrix}, \quad \mathbf{H}_{tu} = \begin{bmatrix} \mathcal{M}_{t1} \mathcal{M}_{u1}^\dagger & \mathcal{M}_{t1} \mathcal{M}_{u2}^\dagger \\ \mathcal{M}_{t2} \mathcal{M}_{u1}^\dagger & \mathcal{M}_{t2} \mathcal{M}_{u2}^\dagger \end{bmatrix}, \quad (26)$$

and the leading order soft matrix as

$$\mathbf{S} = \begin{bmatrix} \theta_1 \theta_1^\dagger & \theta_1 \theta_2^\dagger \\ \theta_2 \theta_1^\dagger & \theta_2 \theta_2^\dagger \end{bmatrix} = \begin{bmatrix} \frac{1}{2} N_c C_F & 0 \\ 0 & N_c^2 \end{bmatrix}, \quad (27)$$

where  $\theta_j^\dagger$  are defined as  $\theta_1^\dagger = (t^a)_{ji} (t^a)_{lk}$  and  $\theta_2^\dagger = \delta_{ji} \delta_{lk}$ . For the  $qq \rightarrow qq$  example, these hard color matrices take the following form

$$\mathbf{H}_{tt} = C_{tt}^u \times 16g_s^4 \frac{N_c}{C_F} \frac{(\hat{s}^2 + \hat{u}^2)}{\hat{t}^2} \begin{bmatrix} 1 & 0 \\ 0 & 0 \end{bmatrix}, \quad (28a)$$

$$\mathbf{H}_{uu} = C_{uu}^u \times 16g_s^4 \frac{1}{N_c C_F} \frac{(\hat{s}^2 + \hat{t}^2)}{\hat{u}^2} \begin{bmatrix} 1 & -C_F \\ -C_F & C_F^2 \end{bmatrix}, \quad (28b)$$

$$\mathbf{H}_{ut} = C_{ut}^u \times 8g_s^4 \frac{N_c}{C_F} \frac{\hat{s}^2}{\hat{t}\hat{u}} \begin{bmatrix} 2 & -C_F \\ -C_F & 0 \end{bmatrix}, \quad (28c)$$

$$\mathbf{H}_{tu} = C_{tu}^u \times 8g_s^4 \frac{N_c}{C_F} \frac{\hat{s}^2}{\hat{t}\hat{u}} \begin{bmatrix} 2 & -C_F \\ -C_F & 0 \end{bmatrix}. \quad (28d)$$

Here the color factors associated with different channels are given by

$$C_{tt}^u = \frac{C_F}{2N_c}, \quad C_{uu}^u = \frac{C_F}{2N_c}, \quad C_{ut}^u = C_{tu}^u = -\frac{C_F}{2N_c^2}. \quad (29)$$

With these color matrices at hand, we immediately obtain the hard functions for different four quark subprocesses,

$$\mathbf{H}_{qq' \rightarrow qq'} = \mathbf{H}_{tt}, \quad \mathbf{H}_{qq' \rightarrow q'q} = \mathbf{H}_{uu}, \quad \mathbf{H}_{qq \rightarrow qq} = \mathbf{H}_{tt} + \mathbf{H}_{uu} + \mathbf{H}_{ut} + \mathbf{H}_{tu}. \quad (30)$$

Summing these matrices gives the hard matrix for  $qq \rightarrow qq$ , which has the following explicit form

$$\mathbf{H}_{qq \rightarrow qq} = \frac{8g_s^4}{t^2 u^2 N_c^2} \begin{bmatrix} t^4 + s^2 t^2 - 2N_c s^2 u t + N_c^2 u^4 + N_c^2 s^2 u^2 & -C_F t (t^3 + s^2 t - N_c s^2 u) \\ -C_F t (t^3 + s^2 t - N_c s^2 u) & C_F^2 t^2 (s^2 + t^2) \end{bmatrix}, \quad (31)$$

which is consistent with the expression below Eq. (46) in [92]. The remaining hard functions can be obtained from crossing symmetries.



12 → 34	Basis	12 → 34	Basis	12 → 34	Basis	12 → 34	Basis	12 → 34	Basis	12 → 34	Basis
$q\bar{q} \rightarrow gg$	$\Gamma_{21}^{ab}$	$qq \rightarrow qq$	$\Gamma_{41}^{ab}$	$qq \rightarrow qq$	$\Gamma_{31}^{ab}$	$qq \rightarrow qq$	$\Gamma_{42}^{ab}$	$qq \rightarrow qq$	$\Gamma_{32}^{ab}$	$gg \rightarrow q\bar{q}$	$\Gamma_{43}^{ab}$
$\bar{q}q \rightarrow \bar{q}q$	$\Gamma_{21}^{ab}$	$\bar{q}q \rightarrow \bar{q}q$	$\Gamma_{41}^{ab}$	$\bar{q}q \rightarrow gg$	$\Gamma_{31}^{ab}$	$gg \rightarrow \bar{q}q$	$\Gamma_{42}^{ab}$	$g\bar{q} \rightarrow \bar{q}g$	$\Gamma_{32}^{ab}$	$g\bar{q} \rightarrow g\bar{q}$	$\Gamma_{43}^{ab}$

TABLE II. The choice of basis for each of two quark two gluon subprocesses.

## 2. Two quarks and two gluon subprocesses

In Tab. II, we provide a list of subprocesses involving two quarks and two gluons with the relevant color bases. We follow the basis choice in Refs. [92–94] by defining the basis operators

$$\Gamma_{1,ij}^{ab} = (t^a t^b)_{ij}, \quad \Gamma_{2,ij}^{ab} = (t^b t^a)_{ij}, \quad \Gamma_{3,ij}^{ab} = \delta_{ij} \delta^{ab}. \quad (32)$$

The corresponding basis is simply given by

$$\theta_1 = (t^a t^b)_{ij}, \quad \theta_2 = (t^b t^a)_{ij}, \quad \theta_3 = \delta_{ij} \delta^{ab}. \quad (33)$$

We note that the normalization of  $\theta_{3,ij}^{ab}$  in [94] differs from the normalization of Refs. [92, 93] by a factor of 2. For our choice of basis, the LO soft matrix is given by

$$\mathbf{S} = \begin{bmatrix} N_c C_F^2 & -\frac{C_F}{2} & N_c C_F \\ -\frac{C_F}{2} & N_c C_F^2 & N_c C_F \\ N_c C_F & N_c C_F & 2N_c^2 C_F \end{bmatrix}. \quad (34)$$

We now provide the expressions for the hard matrices for the  $q\bar{q} \rightarrow gg$  process. This process receives contributions from  $s$ -,  $t$ -,  $u$ -channels and their interference, whose explicit form are given by

$$\mathbf{H}_{tt} = C_{tt}^u \times 4g_s^4 \frac{1}{C_F^3} \frac{(\hat{s}^2 + \hat{t}^2)}{\hat{t}\hat{u}} \begin{bmatrix} 1 & 0 & 0 \\ 0 & 0 & 0 \\ 0 & 0 & 0 \end{bmatrix}, \quad \mathbf{H}_{tu} = C_{tu}^u \times 8g_s^4 \frac{N_c}{C_F^2} \frac{\hat{s}^2}{\hat{t}\hat{u}} \begin{bmatrix} 0 & 1 & 0 \\ 1 & 0 & 0 \\ 0 & 0 & 0 \end{bmatrix}, \quad (35)$$

$$\mathbf{H}_{uu} = C_{uu}^u \times 4g_s^4 \frac{1}{C_F^3} \frac{(\hat{s}^2 + \hat{u}^2)}{\hat{t}\hat{u}} \begin{bmatrix} 0 & 0 & 0 \\ 0 & 1 & 0 \\ 0 & 0 & 0 \end{bmatrix}, \quad \mathbf{H}_{ss} = C_{ss}^u \times 8g_s^4 \frac{1}{C_F^2 N_c} \frac{(\hat{t}^2 + \hat{t}\hat{u} + \hat{u}^2)^2}{\hat{s}^2 \hat{t}\hat{u}} \begin{bmatrix} 1 & -1 & 0 \\ -1 & 1 & 0 \\ 0 & 0 & 0 \end{bmatrix}, \quad (36)$$

$$\mathbf{H}_{st} = C_{st}^u \times 8g_s^2 \frac{1}{C_F^2 N_c} \frac{(2\hat{t} + \hat{u})(\hat{t}^2 + \hat{t}\hat{u} + \hat{u}^2)}{\hat{s}\hat{t}\hat{u}} \begin{bmatrix} 2 & -1 & 0 \\ -1 & 0 & 0 \\ 0 & 0 & 0 \end{bmatrix}, \quad (37)$$

$$\mathbf{H}_{su} = C_{su}^u \times 8g_s^2 \frac{1}{C_F^2 N_c} \frac{(\hat{t} + 2\hat{u})(\hat{t}^2 + \hat{t}\hat{u} + \hat{u}^2)}{\hat{s}\hat{t}\hat{u}} \begin{bmatrix} 0 & -1 & 0 \\ -1 & 2 & 0 \\ 0 & 0 & 0 \end{bmatrix}, \quad (38)$$

where the corresponding color factors are

$$C_{tt}^u = \frac{C_F^2}{N_c}, \quad C_{uu}^u = \frac{C_F^2}{N_c}, \quad C_{tu}^u = -\frac{C_F}{2N_c^2}, \quad C_{ss}^u = C_F, \quad C_{st}^u = \frac{1}{2}C_F, \quad C_{su}^u = \frac{1}{2}C_F. \quad (39)$$

The simplified expression for the hard matrix after sum the sum of all the above matrices is given by

$$\mathbf{H}_{q\bar{q} \rightarrow gg} = 8g_s^4 \frac{(\hat{t}^2 + \hat{u}^2)}{\hat{s}^2} \begin{bmatrix} \frac{\hat{u}}{\hat{t}} & 1 & 0 \\ 1 & \frac{\hat{t}}{\hat{u}} & 0 \\ 0 & 0 & 0 \end{bmatrix}. \quad (40)$$

The hard matrices for other subprocesses involving two quarks and two gluons, such as  $qg \rightarrow qg$ , can be obtained from this expression using crossing symmetries.

### 3. Four gluon subprocesses

For the four gluon subprocesses,  $gg \rightarrow gg$ , we follow the work in Refs. [92, 93] to use the following over-complete basis

$$\begin{aligned} \theta_1 &= \text{Tr} [t^{a_1} t^{a_2} t^{a_3} t^{a_4}] , & \theta_2 &= \text{Tr} [t^{a_1} t^{a_2} t^{a_4} t^{a_3}] , & \theta_3 &= \text{Tr} [t^{a_1} t^{a_4} t^{a_3} t^{a_2}] , \\ \theta_4 &= \text{Tr} [t^{a_1} t^{a_4} t^{a_2} t^{a_3}] , & \theta_5 &= \text{Tr} [t^{a_1} t^{a_3} t^{a_4} t^{a_2}] , & \theta_6 &= \text{Tr} [t^{a_1} t^{a_3} t^{a_2} t^{a_4}] , \\ \theta_7 &= \text{Tr} [t^{a_1} t^{a_4}] \text{Tr} [t^{a_2} t^{a_3}] , & \theta_8 &= \text{Tr} [t^{a_1} t^{a_2}] \text{Tr} [t^{a_3} t^{a_4}] , & \theta_9 &= \text{Tr} [t^{a_1} t^{a_3}] \text{Tr} [t^{a_2} t^{a_4}] . \end{aligned} \quad (41)$$

We note that a six dimensional basis was chosen in [94]. Using this basis in Eq. (41), one can show that the hard matrix takes the following form

$$\mathbf{H}_{gg \rightarrow gg} = \frac{2g_s^4 (\hat{s}^4 + \hat{t}^4 + \hat{u}^4)}{\hat{s}^2 \hat{u}^2 N_c^2 C_F^2} \begin{bmatrix} 1 & \frac{\hat{u}}{\hat{t}} & 1 & \frac{\hat{s}}{\hat{t}} & \frac{\hat{u}}{\hat{t}} & \frac{\hat{s}}{\hat{t}} & 0 & 0 & 0 \\ \frac{\hat{u}}{\hat{t}} & \frac{\hat{u}^2}{\hat{t}^2} & \frac{\hat{u}}{\hat{t}} & \frac{\hat{s}\hat{u}}{\hat{t}^2} & \frac{\hat{u}^2}{\hat{t}^2} & \frac{\hat{s}\hat{u}}{\hat{t}^2} & 0 & 0 & 0 \\ 1 & \frac{\hat{u}}{\hat{t}} & 1 & \frac{\hat{s}}{\hat{t}} & \frac{\hat{u}}{\hat{t}} & \frac{\hat{s}}{\hat{t}} & 0 & 0 & 0 \\ \frac{\hat{s}}{\hat{t}} & \frac{\hat{s}\hat{u}}{\hat{t}^2} & \frac{\hat{s}}{\hat{t}} & \frac{\hat{s}^2}{\hat{t}^2} & \frac{\hat{s}\hat{u}}{\hat{t}^2} & \frac{\hat{s}^2}{\hat{t}^2} & 0 & 0 & 0 \\ \frac{\hat{u}}{\hat{t}} & \frac{\hat{u}^2}{\hat{t}^2} & \frac{\hat{u}}{\hat{t}} & \frac{\hat{s}\hat{u}}{\hat{t}^2} & \frac{\hat{u}^2}{\hat{t}^2} & \frac{\hat{s}\hat{u}}{\hat{t}^2} & 0 & 0 & 0 \\ \frac{\hat{s}}{\hat{t}} & \frac{\hat{s}\hat{u}}{\hat{t}^2} & \frac{\hat{s}}{\hat{t}} & \frac{\hat{s}^2}{\hat{t}^2} & \frac{\hat{s}\hat{u}}{\hat{t}^2} & \frac{\hat{s}^2}{\hat{t}^2} & 0 & 0 & 0 \\ 0 & 0 & 0 & 0 & 0 & 0 & 0 & 0 & 0 \\ 0 & 0 & 0 & 0 & 0 & 0 & 0 & 0 & 0 \\ 0 & 0 & 0 & 0 & 0 & 0 & 0 & 0 & 0 \end{bmatrix} . \quad (42)$$

The LO soft matrix for this channel is given in Appendix C of [93] for this basis as

$$\mathbf{S}_{gg \rightarrow gg} = \frac{C_F}{8N_c} \begin{bmatrix} a_0 & b_0 & c_0 & b_0 & b_0 & b_0 & d_0 & d_0 & -e_0 \\ b_0 & a_0 & b_0 & b_0 & c_0 & b_0 & -e_0 & d_0 & b_0 \\ c_0 & b_0 & a_0 & b_0 & b_0 & b_0 & d_0 & d_0 & -e_0 \\ b_0 & b_0 & b_0 & a_0 & b_0 & c_0 & d_0 & -e_0 & d_0 \\ b_0 & c_0 & b_0 & b_0 & a_0 & b_0 & -e_0 & d_0 & d_0 \\ b_0 & b_0 & b_0 & c_0 & b_0 & a_0 & d_0 & -e_0 & d_0 \\ d_0 & -e_0 & d_0 & d_0 & -e_0 & d_0 & d_0 e_0 & e_0^2 & e_0^2 \\ d_0 & d_0 & d_0 & -e_0 & d_0 & -e_0 & e_0^2 & d_0 e_0 & e_0^2 \\ -e_0 & d_0 & -e_0 & d_0 & d_0 & d_0 & e_0^2 & e_0^2 & d_0 e_0 \end{bmatrix} , \quad (43)$$

where  $a_0 = N_c^4 - 3N_c^2 + 3$ ,  $b_0 = 3 - N_c^2$ ,  $c_0 = 3 + N_c^2$ ,  $d_0 = 2N_c^2 C_F$ , and  $e_0 = N_c$ . We note that for the previous hard matrix calculations, we have separated the contribution from each channel. As we will see, this separation is crucial to computing  $\mathbf{H}^{\text{Sivers}}$ . Since we do not consider the gluon Sivers contributions in this paper, the separation into different channels is not necessary for gluon-gluon subprocess.

## B. Polarized Hard Matrices

As we have emphasized in the previous section, Sivers function is non-universal. The well-known example is the sign change between the Sivers function probed in SIDIS and that in Drell-Yan (DY) process [32–34],

$$f_{1T}^{\perp q(\text{DY})}(x, k_{\perp}, \mu) = -f_{1T}^{\perp q(\text{SIDIS})}(x, k_{\perp}, \mu) . \quad (44)$$

	$tt$	$tu$	$uu$	$ut$
$C^u$	$\frac{C_F}{2N_c}$	$-\frac{C_F}{2N_c^2}$	$\frac{C_F}{2N_c}$	$-\frac{C_F}{2N_c^2}$
$C^i$	$-\frac{1}{2N_c^2}$	$\frac{N_c^2+1}{4N_c^3}$	$-\frac{1}{2N_c^2}$	$\frac{N_c^2+1}{4N_c^3}$
$C^{f_1}$	$-\frac{1}{4N_c^2}$	$\frac{1}{4N_c^3}$	$\frac{N_c^2-2}{4N_c^2}$	$\frac{1}{4N_c^3}$
$C^{f_2}$	$\frac{N_c^2-2}{4N_c^2}$	$\frac{1}{4N_c^3}$	$-\frac{1}{4N_c^2}$	$\frac{1}{4N_c^2}$

TABLE III. Color factors for the  $qq \rightarrow qq$  process

Such a sign change can be easily taken care of in describing the Drell-Yan Sivvers asymmetry,

$$d\Delta\sigma(S_\perp) \propto f_{1T}^{\perp q(\text{DY})}(x, k_\perp, \mu) H(Q, \mu) = f_{1T}^{\perp q(\text{SIDIS})}(x, k_\perp, \mu) [-H(Q, \mu)], \quad (45)$$

where  $H(Q, \mu)$  is the hard function in the Drell-Yan process, and we have applied Eq. (44) in the second step. In other words, if we use the SIDIS Sivvers function in a Drell-Yan process, we shift the minus sign (or the process-dependence) into the hard function.

For the partonic processes in the hadronic dijet production, one has much more complicated process-dependence for the Sivvers functions involved. This can be seen from the highly nontrivial gauge link structure which has been derived in [76] in the definition of the TMD PDFs. It was quickly realized that it would be much easier to incorporate this process-dependence of the Sivvers functions into modified hard functions [43–45, 75, 77], in the same spirit of Eq. (45). We follow a similar procedure in this section to include this process-dependence of the Sivvers functions into the hard functions in the matrix form.

In Fig. 3, we demonstrate the factorization between the Sivvers function and modified hard functions. Unlike the unpolarized case, the contributions of the Sivvers asymmetry are given by considering the attachment of an additional gluon to three of the external legs. Such a gluon is part of the gauge link in the definition of the Sivvers function, and it is the imaginary part of the Feynman diagram (related to the so-called soft gluonic pole) that contributes to the process-dependence of the Sivvers function. We denote these interactions as initial-state ( $i$ ), final-state 1 ( $f_1$ ), and final-state 2 ( $f_2$ ). For each of these cases, there is an associated color factor, denoted as  $C^i$ ,  $C^{f_1}$ ,  $C^{f_2}$  in the figure, which is different for each channel than the unpolarized case (denoted as  $C^u$  in the previous section), while the hard matrix without such a color factor for each channel remains the same. For details, see Ref. [77].

It is important to note that the additional gluon leads to additional complications so that naive crossing symmetry cannot be used to relate one hard function to another, as in the unpolarized case studied above. These complications occur because the contributions to the Sivvers asymmetry are only given by attaching the additional gluon to three of the four external legs. Furthermore, since the sign of the interaction (imaginary part) with the external gluon is opposite for quarks and anti-quarks, this sign must also be accounted for when applying crossing symmetry or charge conjugation.

### 1. Four quark subprocesses

As in the unpolarized case, the bases for four quark subprocesses are given in Tab. I. As we discussed in the previous section, one cannot naively apply crossing symmetry to obtain hard matrices. However, we note that for the four quark subprocesses, when one applies charge conjugation on the polarized cross section, the sign of each color factor only changes by a minus sign. Therefore, the hard matrices for the bottom row of Tab. I can be obtained from the results from the top row of this table with the addition of a minus sign.

We now note that the difference between the polarized and the unpolarized hard functions is only the color factor for these processes. We compute all these color factors and summarize them in Tab. III, which is the same as those in [77]. To calculate the polarized hard matrices, we first use the unpolarized hard matrix and adjust the color factor associated with the interaction to match the polarized case. Here we explicitly perform the calculation for the hard matrix for the  $qq \rightarrow qq$  subprocess. Later, we provide the expressions for each of the remaining subprocesses. The polarized hard matrix for  $qq' \rightarrow qq'$  ( $t$ -channel) and  $qq' \rightarrow q'q$  ( $u$ -channel) can be obtained

$$\mathbf{H}_{qq' \rightarrow qq'}^{\text{Sivvers}} = \frac{C_{tt}^i + C_{tt}^{f_1} + C_{tt}^{f_2}}{C_{tt}^u} \mathbf{H}_{tt} = 4g_s^4 \frac{(N_c^2 - 5)}{C_F N_c} \frac{(\hat{s}^2 + \hat{u}^2)}{\hat{t}^2} \begin{bmatrix} 1 & 0 \\ 0 & 0 \end{bmatrix}, \quad (46)$$

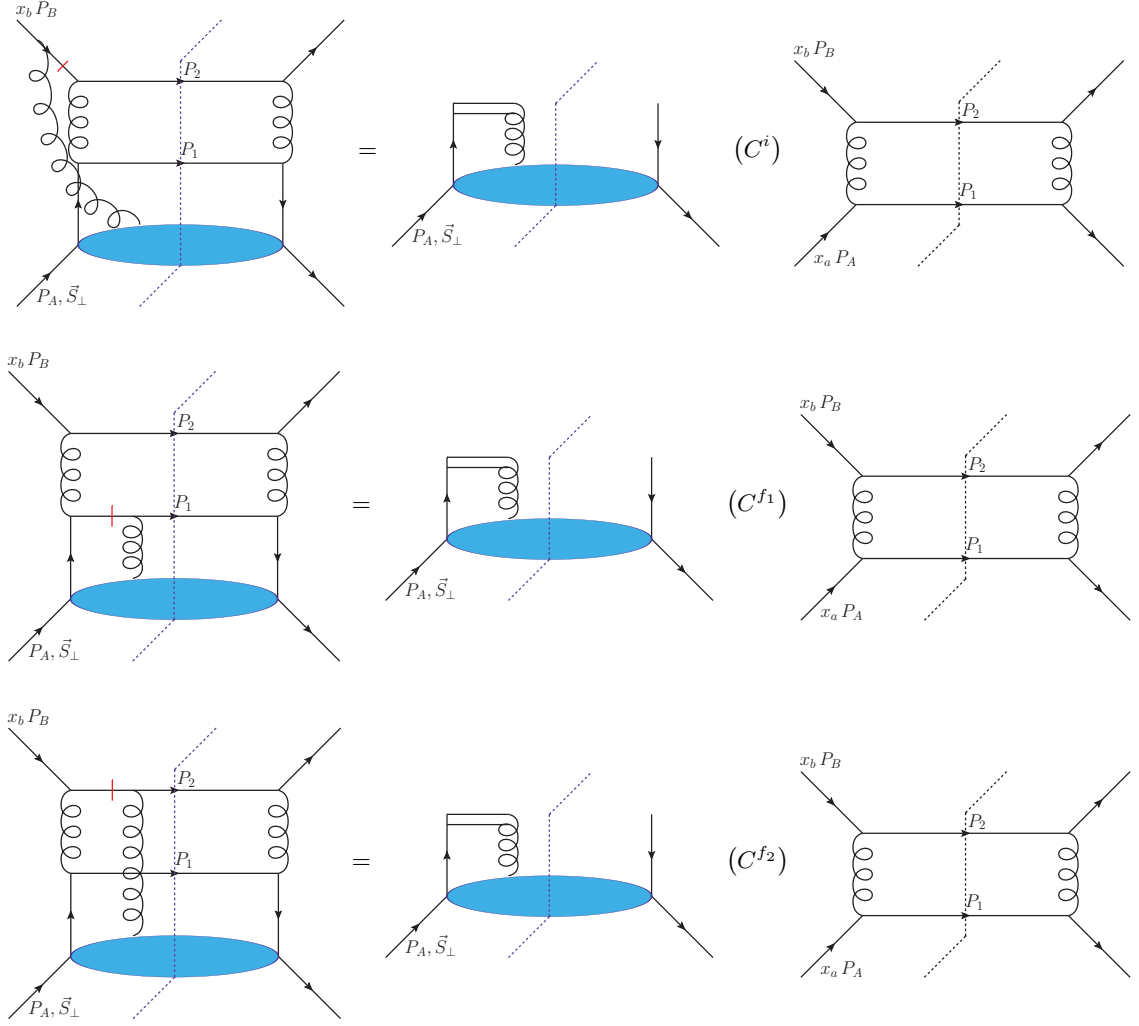


FIG. 3. A demonstration of the factorization between the Siverson function and the hard function for the process  $qq' \rightarrow qq'$ . From top to bottom, we provide the diagrams for the initial-state interaction, final-state 1 interaction, and final-state 2 interaction. The red lines indicate the locations of the soft poles. The color factors  $C^i$ ,  $C^{f1}$ , and  $C^{f2}$  contain the process-dependence of these interactions. Once isolating these color factors, the remaining hard function is defined to be independent of this color flow.

$$\mathbf{H}_{qq' \rightarrow qq'}^{\text{Sivers}} = \frac{C_{uu}^i + C_{uu}^{f1} + C_{uu}^{f2}}{C_{uu}^u} \mathbf{H}_{uu} = 4g_s^4 \frac{(N_c^2 - 5)}{N_c^3 C_F} \frac{(\hat{s}^2 + \hat{t}^2)}{\hat{u}^2} \begin{bmatrix} 1 & -C_F \\ -C_F & C_F^2 \end{bmatrix}, \quad (47)$$

where the matrix form for  $\mathbf{H}_{tt}$  and  $\mathbf{H}_{uu}$  are given in Eq. (28), and the relevant color factors are summarized in Tab. III. On the other hand, for  $qq \rightarrow qq$  subprocess, since it receives contributions from both  $t$ - and  $u$ -channels (as well as their interference), the structure is more complicated,

$$\begin{aligned} \mathbf{H}_{qq \rightarrow qq}^{\text{Sivers}} &= \frac{C_{uu}^i + C_{uu}^{f1} + C_{uu}^{f2}}{C_{uu}^u} \mathbf{H}_{uu} + \frac{C_{tt}^i + C_{tt}^{f1} + C_{tt}^{f2}}{C_{tt}^u} \mathbf{H}_{tt} + \frac{C_{tu}^i + C_{tu}^{f1} + C_{tu}^{f2}}{C_{tu}^u} (\mathbf{H}_{tu} + \mathbf{H}_{ut}), \\ &= \mathbf{H}_{qq' \rightarrow qq'}^{\text{Sivers}} + \mathbf{H}_{qq' \rightarrow q'q}^{\text{Sivers}} + 4g_s^4 \frac{(N_c^2 + 3)}{N_c^2 C_F} \frac{\hat{s}^2}{\hat{t}\hat{u}} \begin{bmatrix} 2 & -C_F \\ -C_F & 0 \end{bmatrix}. \end{aligned} \quad (48)$$

One can show that after performing the trace with the soft color matrix, that the expressions for the polarized hard functions are consistent with [77]. The color matrices for the remaining four quark subprocesses can be computed in

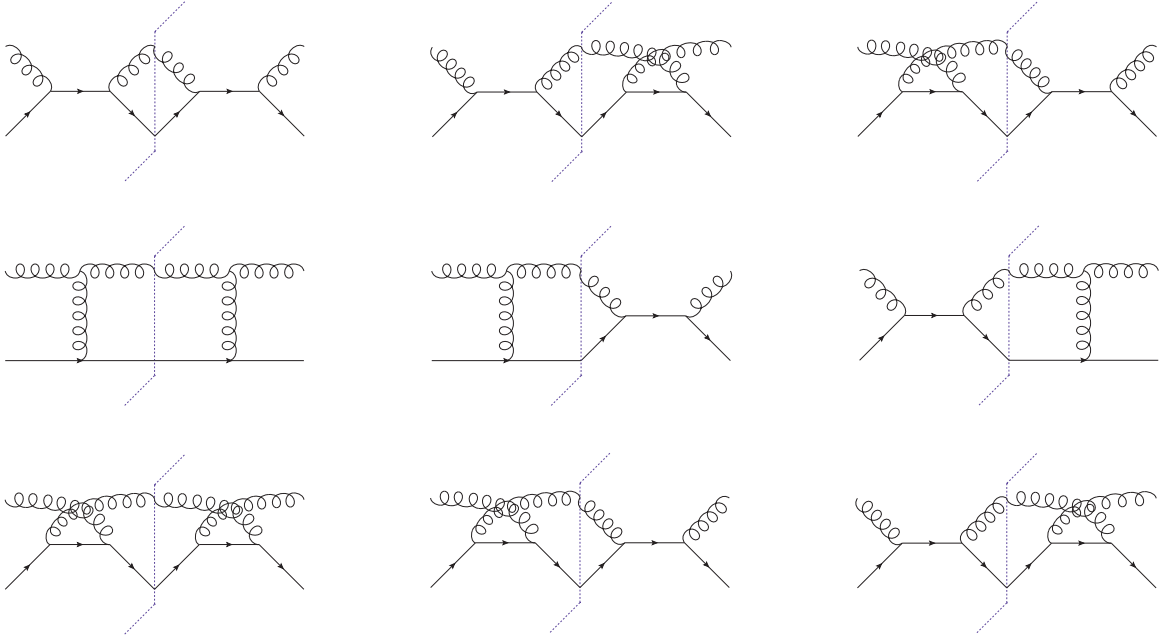


FIG. 4. Each of the leading order diagrams for  $q\bar{q} \rightarrow q\bar{q}$ . For the Siverson function, an additional gluon is attached at three of the external legs as in Fig. 3. This results in 18 independent color factors for this subprocess. All other subprocesses in Tab. II will also have 18 independent color factors.

the same way to obtain the following expressions

$$\mathbf{H}_{q\bar{q} \rightarrow q'\bar{q}'}^{\text{Sivers}} = 4g_s^4 \frac{(N_c^2 + 1)}{N_c C_F} \frac{(\hat{t}^2 + \hat{u}^2)}{\hat{s}^2} \begin{bmatrix} 1 & 0 \\ 0 & 0 \end{bmatrix}, \quad (49)$$

$$\mathbf{H}_{q\bar{q}' \rightarrow q\bar{q}'}^{\text{Sivers}} = -4g_s^4 \frac{(N_c^2 - 3)}{N_c^3 C_F} \frac{(\hat{s}^2 + \hat{u}^2)}{\hat{t}^2} \begin{bmatrix} 1 & -C_F \\ -C_F & C_F^2 \end{bmatrix}, \quad (50)$$

$$\mathbf{H}_{q\bar{q} \rightarrow q\bar{q}}^{\text{Sivers}} = \mathbf{H}_{q\bar{q} \rightarrow q'\bar{q}'}^{\text{Sivers}} + \mathbf{H}_{q\bar{q}' \rightarrow q\bar{q}'}^{\text{Sivers}} - 4g_s^4 \frac{(N_c^2 + 1)}{N_c^2 C_F} \frac{\hat{u}^2}{\hat{s}\hat{t}} \begin{bmatrix} 2 & -C_F \\ -C_F & 0 \end{bmatrix}, \quad (51)$$

$$\mathbf{H}_{q\bar{q}' \rightarrow \bar{q}'q}^{\text{Sivers}} = -4g_s^4 \frac{(N_c^2 - 3)}{C_F N_c} \frac{(\hat{s}^2 + \hat{t}^2)}{\hat{u}^2} \begin{bmatrix} 1 & 0 \\ 0 & 0 \end{bmatrix}, \quad (52)$$

$$\mathbf{H}_{q\bar{q} \rightarrow \bar{q}'q'}^{\text{Sivers}} = 4g_s^4 \frac{(N_c^2 + 1)}{N_c^3 C_F} \frac{(\hat{t}^2 + \hat{u}^2)}{\hat{s}^2} \begin{bmatrix} 1 & -C_F \\ -C_F & C_F^2 \end{bmatrix}, \quad (53)$$

$$\mathbf{H}_{q\bar{q} \rightarrow q\bar{q}}^{\text{Sivers}} = \mathbf{H}_{q\bar{q}' \rightarrow \bar{q}'q}^{\text{Sivers}} + \mathbf{H}_{q\bar{q} \rightarrow \bar{q}'q'}^{\text{Sivers}} - 4g_s^4 \frac{(N_c^2 + 1)}{N_c^2 C_F} \frac{\hat{t}^2}{\hat{s}\hat{u}} \begin{bmatrix} 2 & -C_F \\ -C_F & 0 \end{bmatrix}. \quad (54)$$

After performing charge conjugation, the hard color matrices for the remaining subprocesses can be obtained from these expressions.

## 2. Two quarks and two gluon subprocesses

All twelve of the two quark and two gluon subprocesses are given in Tab. II. As we have mentioned in Introduction, we neglect the gluon Siverson contribution in this paper. This means that all subprocesses with a gluon incoming from the polarized proton will be neglected. There are then six remaining subprocesses to compute. While in the previous

	$ss$	$st$	$ts$	$tt$	$tu$	$ut$	$uu$	$us$	$su$
$C^u$	$\frac{C_F}{2N_c}$	$\frac{1}{4}$	$\frac{1}{4}$	$\frac{1}{2}$	$-\frac{1}{4}$	$-\frac{1}{4}$	$\frac{C_F}{2N_c}$	$-\frac{1}{4N_c}$	$-\frac{1}{4N_c}$
$C^i$	$-\frac{1}{4}$	$-\frac{N_c^2}{4(N_c^2-1)}$	$-\frac{N_c^2}{4(N_c^2-1)}$	$-\frac{N_c^2}{4(N_c^2-1)}$	0	0	$\frac{1}{4(N_c^2-1)}$	$\frac{1}{4(N_c^2-1)}$	$\frac{1}{4(N_c^2-1)}$
$C^{f_1}$	$\frac{1}{4(N_c^2-1)N_c^2}$	$-\frac{1}{4(N_c^2-1)}$	$-\frac{1}{4(N_c^2-1)}$	$-\frac{1}{2(N_c^2-1)}$	$\frac{1}{4(N_c^2-1)}$	$\frac{1}{4(N_c^2-1)}$	$\frac{1}{4(N_c^2-1)N_c^2}$	$\frac{N_c^2+1}{4(N_c^2-1)N_c^2}$	$\frac{N_c^2+1}{4(N_c^2-1)N_c^2}$
$C^{f_2}$	$-\frac{1}{4(N_c^2-1)}$	0	0	$\frac{N_c^2}{4(N_c^2-1)}$	$-\frac{N_c^2}{4(N_c^2-1)}$	$-\frac{N_c^2}{4(N_c^2-1)}$	$\frac{1}{4}$	$-\frac{1}{4(N_c^2-1)}$	$-\frac{1}{4(N_c^2-1)}$

TABLE IV. Color factors for the  $q\bar{q} \rightarrow q\bar{q}$  process. There are in total 27 color factors for 9 channels  $\mathbf{H}_{ss}, \mathbf{H}_{st}, \mathbf{H}_{ts}, \mathbf{H}_{tt}, \mathbf{H}_{tu}, \mathbf{H}_{ut}, \mathbf{H}_{uu}, \mathbf{H}_{us}, \mathbf{H}_{su}$ , respectively. However, we notice that the interference channels,  $st$  vs  $ts$ ,  $tu$  vs  $ut$ , and  $us$  vs  $su$ , have the same color factors. Thus in total we have 18 independent color factors.

section, we were able to relate the hard matrices for the quark and anti-quark channels, the argument that we gave in the previous section is no longer valid. This issue occurs because the sign of the color factors for the external gluon attaching to a gluon leg does not change by a minus sign under charge conjugation. We must then compute the hard matrices for the quark and anti-quark subprocesses separately. Therefore there are six subprocesses to be computed. We note that for each of these subprocesses, there are nine possible channels corresponding to the natural Mandelstam variables that describe the channel. Each of these channels has three unique color factors which must be computed. In Fig. 4, we provide all the 9 diagrams ( $ss, st, ts, tt, tu, ut, uu, us, su$ ) in  $q\bar{q} \rightarrow q\bar{q}$  subprocess as an example, and the additional gluon can be attached into three places for each of such diagrams, which leads to 27 color factors, although only 18 of them are independent ones since the interference diagrams give the same colors ( $st$  vs  $ts$ ,  $ut$  vs  $tu$ , and  $us$  vs  $su$ ). These color factors are summarized in Tab. IV.

To compute the hard matrices for the example  $q\bar{q} \rightarrow q\bar{q}$  subprocess, following the same procedure as in the four quark case, we write

$$\mathbf{H}_{q\bar{q} \rightarrow q\bar{q}}^{\text{Sivers}} = \frac{C_{ss}^i + C_{ss}^{f_1} + C_{ss}^{f_2}}{C_{ss}^u} \mathbf{H}_{q\bar{q} \rightarrow q\bar{q}, ss} + \frac{C_{st}^i + C_{st}^{f_1} + C_{st}^{f_2}}{C_{st}^u} (\mathbf{H}_{q\bar{q} \rightarrow q\bar{q}, st} + \mathbf{H}_{q\bar{q} \rightarrow q\bar{q}, ts}) \quad (55)$$

$$+ \frac{C_{tt}^i + C_{tt}^{f_1} + C_{tt}^{f_2}}{C_{tt}^u} \mathbf{H}_{q\bar{q} \rightarrow q\bar{q}, tt} + \frac{C_{tu}^i + C_{tu}^{f_1} + C_{tu}^{f_2}}{C_{tu}^u} (\mathbf{H}_{q\bar{q} \rightarrow q\bar{q}, tu} + \mathbf{H}_{q\bar{q} \rightarrow q\bar{q}, ut})$$

$$+ \frac{C_{uu}^i + C_{uu}^{f_1} + C_{uu}^{f_2}}{C_{uu}^u} \mathbf{H}_{q\bar{q} \rightarrow q\bar{q}, uu} + \frac{C_{us}^i + C_{us}^{f_1} + C_{us}^{f_2}}{C_{us}^u} (\mathbf{H}_{q\bar{q} \rightarrow q\bar{q}, us} + \mathbf{H}_{q\bar{q} \rightarrow q\bar{q}, su}), \quad (56)$$

where the subscript is again associated with the Madelstam variables for the channels that contribute to the subprocess. The final expressions for these functions become quite complicated because of the number of contributions. After taking  $N_c = 3$  and  $C_F = 4/3$ , the polarized hard matrices for these subprocesses are given by

$$\mathbf{H}_{q\bar{q} \rightarrow q\bar{q}}^{\text{Sivers}} = \frac{g_s^4}{4\hat{s}\hat{t}^2\hat{u}} \begin{bmatrix} -8(9\hat{t}^4 + 18\hat{u}\hat{t}^3 + 22\hat{u}^2\hat{t}^2 + 8\hat{u}^3\hat{t} - \hat{u}^4) & 8\hat{u}(13\hat{t}^3 + 12\hat{u}\hat{t}^2 + 7\hat{u}^2\hat{t} - \hat{u}^3) & 0 \\ 8\hat{u}(13\hat{t}^3 + 12\hat{u}\hat{t}^2 + 7\hat{u}^2\hat{t} - \hat{u}^3) & 31\hat{t}^4 + 16\hat{u}\hat{t}^3 - 17\hat{u}^2\hat{t}^2 - 48\hat{u}^3\hat{t} + 8\hat{u}^4 & 0 \\ 0 & 0 & 0 \end{bmatrix}, \quad (57)$$

$$\mathbf{H}_{q\bar{q} \rightarrow q\bar{q}}^{\text{Sivers}} = \frac{g_s^4}{4\hat{s}\hat{t}\hat{u}^2} \begin{bmatrix} 8(\hat{t}^4 - 8\hat{u}\hat{t}^3 - 22\hat{u}^2\hat{t}^2 - 18\hat{u}^3\hat{t} - 9\hat{u}^4) & -8\hat{t}(\hat{t}^3 - 7\hat{u}\hat{t}^2 - 12\hat{u}^2\hat{t} - 13\hat{u}^3) & 0 \\ -8\hat{t}(\hat{t}^3 - 7\hat{u}\hat{t}^2 - 12\hat{u}^2\hat{t} - 13\hat{u}^3) & 8\hat{t}^4 - 48\hat{u}\hat{t}^3 - 17\hat{u}^2\hat{t}^2 + 16\hat{u}^3\hat{t} + 31\hat{u}^4 & 0 \\ 0 & 0 & 0 \end{bmatrix}, \quad (58)$$

$$\mathbf{H}_{q\bar{q} \rightarrow q\bar{q}}^{\text{Sivers}} = \frac{g_s^4}{4\hat{s}^2\hat{t}\hat{u}} \begin{bmatrix} -178\hat{s}^4 - 258\hat{u}\hat{s}^3 - 209\hat{u}^2\hat{s}^2 + 80\hat{u}^4 & -16(2\hat{s}^4 - 5\hat{u}\hat{s}^3 + 5\hat{u}^3\hat{s} + 5\hat{u}^4) & 0 \\ -16(2\hat{s}^4 - 5\hat{u}\hat{s}^3 + 5\hat{u}^3\hat{s} + 5\hat{u}^4) & 111\hat{t}^4 + 284\hat{u}\hat{t}^3 + 457\hat{u}^2\hat{t}^2 + 346\hat{u}^3\hat{t} + 142\hat{u}^4 & 0 \\ 0 & 0 & 0 \end{bmatrix}, \quad (59)$$

$$\mathbf{H}_{q\bar{q} \rightarrow q\bar{q}}^{\text{Sivers}} = \frac{g_s^4}{4\hat{s}\hat{t}^2\hat{u}} \begin{bmatrix} 8(4\hat{t}^4 - 2\hat{u}\hat{t}^3 - 8\hat{u}^2\hat{t}^2 - 12\hat{u}^3\hat{t} - \hat{u}^4) & -8\hat{s}(9\hat{t}^3 + 5\hat{u}\hat{t}^2 + 10\hat{u}^2\hat{t} + \hat{u}^3) & 0 \\ -8\hat{s}(9\hat{t}^3 + 5\hat{u}\hat{t}^2 + 10\hat{u}^2\hat{t} + \hat{u}^3) & -54\hat{t}^4 - 126\hat{u}\hat{t}^3 - 175\hat{u}^2\hat{t}^2 - 80\hat{u}^3\hat{t} - 8\hat{u}^4 & 0 \\ 0 & 0 & 0 \end{bmatrix}, \quad (60)$$

$$\mathbf{H}_{\bar{q}g \rightarrow g\bar{q}}^{\text{Sivers}} = -\frac{g_s^4}{4\hat{s}\hat{t}\hat{u}^2} \begin{bmatrix} 8(\hat{t}^4 + 12\hat{u}\hat{t}^3 + 8\hat{u}^2\hat{t}^2 + 2\hat{u}^3\hat{t} - 4\hat{u}^4) & 8\hat{s}(\hat{t}^3 + 10\hat{u}\hat{t}^2 + 5\hat{u}^2\hat{t} + 9\hat{u}^3) & 0 \\ 8\hat{s}(\hat{t}^3 + 10\hat{u}\hat{t}^2 + 5\hat{u}^2\hat{t} + 9\hat{u}^3) & 8\hat{t}^4 + 80\hat{u}\hat{t}^3 + 175\hat{u}^2\hat{t}^2 + 126\hat{u}^3\hat{t} + 54\hat{u}^4 & 0 \\ 0 & 0 & 0 \end{bmatrix}, \quad (61)$$

$$\mathbf{H}_{\bar{q}q \rightarrow gq}^{\text{Sivers}} = \frac{8g_s^4}{\hat{s}^2\hat{t}\hat{u}} \begin{bmatrix} 3\hat{t}^4 + 8\hat{u}\hat{t}^3 + 13\hat{u}^2\hat{t}^2 + 10\hat{u}^3\hat{t} + 4\hat{u}^4 & \hat{t}^4 + 2\hat{u}\hat{t}^3 - \hat{u}^4 & 0 \\ \hat{t}^4 + 2\hat{u}\hat{t}^3 - \hat{u}^4 & -4\hat{s}^4 - 6\hat{u}\hat{s}^3 - 5\hat{u}^2\hat{s}^2 + 2\hat{u}^4 & 0 \\ 0 & 0 & 0 \end{bmatrix}. \quad (62)$$

### C. Evolution equations

Hard functions can be related to the Wilson coefficients  $C_I^\Gamma$  in the color basis  $\{\theta_I\}$  of section III by  $H_{IJ} = \sum_\Gamma C_I^\Gamma C_J^{\Gamma*}$ . Here  $\Gamma$  represents different helicity states of the incoming and outgoing particles. Explicit expressions of the Wilson coefficients at next-to-leading order can be found in [92, 93], but we do not present them as we are only using the tree-level hard functions for our study. We do, however, include the renormalization group (RG) evolution of the hard functions coming from the 1-loop anomalous dimensions. Then the Wilson coefficients satisfy the RG evolution equations [92, 93, 95, 96]

$$\mu \frac{d}{d\mu} C_I^\Gamma = \left[ \left( \gamma_{\text{cusp}} \frac{c_H}{2} \ln \frac{-\hat{t}}{\mu^2} + \gamma_H \right) \delta_{IJ} + \gamma_{\text{cusp}} M_{IJ} \right] C_J^\Gamma. \quad (63)$$

Here,  $\gamma_{\text{cusp}} = \frac{\alpha_s}{\pi} + \dots$  is the cusp anomalous dimensions and  $c_H = C_a + C_b + C_c + C_d$ . The non-cusp anomalous dimension is defined as

$$\gamma_H = -\frac{1}{2} \left( \gamma_\mu^a [\alpha_s(\mu)] + \gamma_\mu^b [\alpha_s(\mu)] + \gamma_\mu^c [\alpha_s(\mu)] + \gamma_\mu^d [\alpha_s(\mu)] \right), \quad (64)$$

where  $\gamma_\mu^i [\alpha_s(\mu)] = \frac{\alpha_s}{\pi} \gamma_i + \dots$ , with  $\gamma_q = \frac{3}{2} C_F$  and  $\gamma_g = \frac{\beta_0}{2}$ . Lastly, the matrix  $\mathbf{M}$  takes the form

$$\mathbf{M} = -\sum_{i < j} \mathbf{T}_i \cdot \mathbf{T}_j [L(s_{ij}) - L(\hat{t})], \quad (65)$$

where  $s_{12} = s_{34} = \hat{s}$ ,  $s_{13} = s_{24} = \hat{t}$ , and  $s_{14} = s_{23} = \hat{u}$  and

$$L(\hat{t}) = \ln \left( \frac{-\hat{t}}{\mu^2} \right), \quad L(\hat{u}) = \ln \left( \frac{-\hat{u}}{\mu^2} \right), \quad L(\hat{s}) = \ln \left( \frac{\hat{s}}{\mu^2} \right) - i\pi. \quad (66)$$

From the RG evolution of the Wilson coefficients given in Eq. (63), we can arrive at the RG evolution equations for  $\mathbf{H}$  as

$$\mu \frac{d}{d\mu} \mathbf{H} = \mathbf{\Gamma}^H \cdot \mathbf{H} + \mathbf{H} \cdot \mathbf{\Gamma}^{H\dagger}, \quad (67)$$

where  $\mathbf{\Gamma}^H$  is given by

$$\mathbf{\Gamma}^H = \left( \gamma_{\text{cusp}} \frac{c_H}{2} \ln \frac{-\hat{t}}{\mu^2} + \gamma_H \right) \mathbf{I} + \gamma_{\text{cusp}} \mathbf{M}. \quad (68)$$

## IV. QCD RESUMMATION AND EVOLUTION FORMALISM

In this section, we present the renormalization group (RG) equations for the rest key ingredients in the factorized formalism. These include the TMD PDFs, global soft functions, jet functions, and collinear-soft functions. After presenting their NLO perturbative results and RG evolution equations, we check the RG consistency. In the end, we present our resummation formula for dijet production in both unpolarized and polarized scatterings.

### A. TMDs and global soft functions

The unsubtracted TMD PDFs in the factorized formula in Eq. (6) describe the radiation along the incoming beams. They satisfy the RG evolution equations

$$\mu \frac{d}{d\mu} \ln f_i^{\text{unsub}}(x, b, \mu, \nu) = \gamma_\mu^{f_i}(\mu, \nu), \quad (69)$$

$$\nu \frac{d}{d\nu} \ln f_i^{\text{unsub}}(x, b, \mu, \nu) = \gamma_\nu^{f_i}(\mu), \quad (70)$$

where its  $\mu$ - and  $\nu$ -anomalous dimensions are given by

$$\gamma_\mu^{f_i}(\mu, \nu) = \gamma_{\text{cusp}} C_i \ln \frac{\nu^2}{x_i^2 P^{-2}} + \gamma_\mu^i[\alpha_s(\mu)], \quad (71)$$

$$\gamma_\nu^{f_i}(\mu, \nu) = \frac{\alpha_s C_i}{\pi} \ln \frac{\mu^2}{\mu_b^2}. \quad (72)$$

As we will see in this subsection, the rapidity divergences of the unsubtracted TMDs will be exactly canceled by the rapidity divergences of the global soft functions, which will allow us to identify the standard TMDs with subtracted rapidity divergence as in Eq. (8) above.

Suppressing the label  $ab \rightarrow cd$  for convenience, the global soft functions up to 1-loop are given by

$$\mathbf{S}^{(0)}(b) = \mathbf{I}, \quad (73)$$

$$\mathbf{S}^{\text{bare},(1)}(b) = \sum_{i < j} \mathbf{T}_i \cdot \mathbf{T}_j \mathcal{I}_{ij}^{(1)}(b), \quad (74)$$

where [97]

$$\mathcal{I}_{12}^{(1)}(b) = \frac{\alpha_s}{2\pi} \left[ 2 \left( \frac{2}{\eta} + \ln \frac{\nu^2}{\mu^2} \right) \left( \frac{1}{\epsilon} + \ln \frac{\mu^2}{\mu_b^2} \right) - \frac{2}{\epsilon^2} + \ln^2 \frac{\mu^2}{\mu_b^2} + \frac{\pi^2}{6} \right], \quad (75)$$

$$\mathcal{I}_{13}^{(1)}(b) = \frac{\alpha_s}{2\pi} \left[ \left( \frac{2}{\eta} + \ln \frac{\nu^2}{\mu^2} - 2y_c \right) \left( \frac{1}{\epsilon} + \ln \frac{\mu^2}{\mu_b^2} \right) - \frac{2}{\epsilon^2} - \frac{1}{\epsilon} \ln \frac{\mu^2}{\mu_b^2} + \frac{\pi^2}{6} \right], \quad (76)$$

$$\mathcal{I}_{34}^{(1)}(b) = \frac{\alpha_s}{2\pi} \left[ 4 \left( \frac{1}{\epsilon} + \ln \frac{\mu^2}{\mu_b^2} \right) \ln(2 \cosh(\Delta y/2)) - \frac{2}{\epsilon^2} - \frac{2}{\epsilon} \ln \frac{\mu^2}{\mu_b^2} - \ln^2 \frac{\mu^2}{\mu_b^2} + \Delta y^2 - 4 \ln^2(2 \cosh(\Delta y/2)) + \frac{\pi^2}{6} \right], \quad (77)$$

$$\mathcal{I}_{14}^{(1)}(b) = \mathcal{I}_{13}^{(1)}(b)(y_c \rightarrow y_d), \quad \mathcal{I}_{23}^{(1)}(b) = \mathcal{I}_{13}^{(1)}(b)(y_c \rightarrow -y_c), \quad \mathcal{I}_{24}^{(1)}(b) = \mathcal{I}_{14}^{(1)}(b)(y_d \rightarrow -y_d). \quad (78)$$

The explicit matrix forms of tree-level soft functions in Eq. (73) for some color basis  $\{\theta_I\}$  can be computed as

$$(I)_{IJ} = \theta_I \theta_J^\dagger, \quad (79)$$

which is equivalent to the matrix forms of the LO soft functions found in section III. The matrix  $\mathbf{T}_i \cdot \mathbf{T}_j$  of the eq. (74) was also computed in the same color basis and can be found in [92, 93]. The renormalized global soft functions satisfy the RG evolution equations

$$\mu \frac{d}{d\mu} \mathbf{S}(b, \mu, \nu) = \mathbf{\Gamma}_\mu^{S\dagger} \cdot \mathbf{S} + \mathbf{S} \cdot \mathbf{\Gamma}_\mu^S, \quad (80)$$

$$\nu \frac{d}{d\nu} \mathbf{S}(b, \mu, \nu) = \mathbf{\Gamma}_\nu^{S\dagger} \cdot \mathbf{S} + \mathbf{S} \cdot \mathbf{\Gamma}_\nu^S, \quad (81)$$

$$(82)$$

From Eqs. (73) - (78) and using  $\sum_i \mathbf{T}_i = 0$ , we then find

$$\begin{aligned} \mathbf{\Gamma}_\mu^S = & -\frac{\alpha_s}{2\pi} \left[ C_a \left( \ln \frac{-\hat{t}}{x_a^2 S} + \ln \frac{\nu^2}{\mu^2} \right) + C_b \left( \ln \frac{-\hat{t}}{x_b^2 S} + \ln \frac{\nu^2}{\mu^2} \right) + (C_c + C_d) \left( \ln \frac{-\hat{t}}{P_1^2} - \ln \frac{\mu^2}{\mu_b^2} \right) \right] \mathbf{I} \\ & - \frac{\alpha_s}{\pi} \mathbf{M} + \frac{\alpha_s}{\pi} (\mathbf{T}_1 \cdot \mathbf{T}_2 + \mathbf{T}_3 \cdot \mathbf{T}_4) i\pi \end{aligned}$$



$$\begin{aligned}
&= -\frac{\gamma_{\text{cusp}}}{2} \left[ C_a \left( \ln \frac{-\hat{t}}{x_a^2 S} + \ln \frac{\nu^2}{\mu^2} \right) + C_b \left( \ln \frac{-\hat{t}}{x_b^2 S} + \ln \frac{\nu^2}{\mu^2} \right) + (C_c + C_d) \left( \ln \frac{-\hat{t}}{P_\perp^2} - \ln \frac{\mu^2}{\mu_b^2} \right) \right] \mathbf{I} \\
&\quad - \gamma_{\text{cusp}} \mathbf{M} + \gamma_{\text{cusp}} (\mathbf{T}_1 \cdot \mathbf{T}_2 + \mathbf{T}_3 \cdot \mathbf{T}_4) i\pi,
\end{aligned} \tag{83}$$

$$\mathbf{\Gamma}_\nu^S = -\frac{\alpha_s(C_a + C_b)}{2\pi} \ln \frac{\mu^2}{\mu_b^2} \mathbf{I}, \tag{84}$$

where  $\mathbf{M}$  was given in Eq. (65) and we promoted  $\frac{\alpha_s}{\pi} \rightarrow \gamma_{\text{cusp}}$ , which is consistent with the factorization consistency relation below. Note that Eq. (83) is strictly real and the imaginary term  $\sim i\pi$  cancels exactly with the imaginary term found in  $\mathbf{M}$ .

We note that  $\mathbf{\Gamma}_\nu^S \sim \mathbf{I}$  and that this is expected as the hard functions do not have any rapidity divergence. Thus, we can write

$$\nu \frac{d}{d\nu} \mathbf{S}(b, \mu, \nu) = \mathbf{\Gamma}_\nu^{S\dagger} \cdot \mathbf{S} + \mathbf{S} \cdot \mathbf{\Gamma}_\nu^S = -\frac{\alpha_s(C_a + C_b)}{\pi} \ln \frac{\mu^2}{\mu_b^2} \mathbf{S}(b, \mu, \nu), \tag{85}$$

which has the same rapidity anomalous dimensions as the back-to-back soft functions  $S_{ab}(b, \mu, \nu)$  found in standard Drell-Yan and SIDIS process [67]. As expected, the rapidity divergence of the global soft function  $\mathbf{S}(b, \mu, \nu)$  in Eq. (85) exactly cancels the rapidity anomalous dimensions for the unsubtracted TMDs  $f_a(b, \mu, \nu)$  and  $f_b(b, \mu, \nu)$  given in Eq. (72). Therefore, as discussed in the introduction, we can define  $\tilde{\mathbf{S}}(b, \mu)$  absent of the rapidity divergence such that

$$\mathbf{S}(b, \mu, \nu) = \tilde{\mathbf{S}}(b, \mu) S_{ab}(b, \mu, \nu). \tag{86}$$

Then as in Eq. (8),  $S_{ab}(b, \mu, \nu)$  is combined with the unsubtracted TMDs to identify standard TMDs free of the rapidity divergences.

## B. Jet and collinear-soft functions

Both jet and collinear-soft functions describe the radiation which resolves the produced jets. The jet functions [98, 99] encode the collinear radiations inside anti- $k_T$  jet with radius  $R$ . The NLO expressions are given by

$$J_i(P_\perp R, \mu) = 1 + \frac{\alpha_s}{\pi} \left[ \frac{C_i}{4} \ln^2 \left( \frac{\mu^2}{P_\perp^2 R^2} \right) + \frac{\gamma_i}{2} \ln \left( \frac{\mu^2}{P_\perp^2 R^2} \right) + d_i \right], \tag{87}$$

where the algorithmic dependent terms  $d_i$  for anti- $k_T$  algorithm are

$$d_q = \left( \frac{13}{4} - \frac{3\pi^2}{8} \right) C_F, \tag{88}$$

$$d_g = \left( \frac{67}{18} - \frac{3\pi^2}{8} \right) C_A - \frac{23}{36} n_f. \tag{89}$$

The jet functions satisfy the RG evolution equations

$$\mu \frac{d}{d\mu} J_i(P_\perp R, \mu) = \gamma_\mu^{J_i}(\mu) J_i(P_\perp R, \mu), \tag{90}$$

where the anomalous dimension is given by

$$\gamma_\mu^{J_i}(\mu) = \gamma_{\text{cusp}} C_i \ln \left( \frac{\mu^2}{P_\perp^2 R^2} \right) + \gamma_\mu^i[\alpha_s(\mu)]. \tag{91}$$

The collinear-soft functions [55, 56] describe the soft radiation along the jet direction and resolves the jet cone  $R$ . The NLO expressions are given by

$$S_i^{cs,(1)}(b, R, \mu) = 1 - \frac{\alpha_s C_i}{4\pi} \left[ \ln^2 \left( \frac{\mu^2}{\mu_b^2 R^2} \right) - \frac{\pi^2}{6} \right]. \tag{92}$$

The collinear-soft functions satisfy the RG evolution equations

$$\mu \frac{d}{d\mu} S_i^{\text{cs}}(b, R, \mu) = \gamma_\mu^{\text{cs}_i}(\mu) S_i^{\text{cs}}(b, R, \mu), \quad (93)$$

where its anomalous dimension takes the form

$$\gamma_\mu^{\text{cs}_i}(\mu) = \gamma_{\text{cusp}} C_i \ln \left( \frac{\mu^2}{\mu_b^2 R^2} \right). \quad (94)$$

### C. RG consistency at 1-loop

With the anomalous dimensions presented for all the ingredients, we now show that our factorized formula given in Eq. (6) satisfy the consistency relations for the RG evolutions. The cancellation of the rapidity divergences was already checked around Eq. (85). We also expect  $\mu$ -divergence of the various functions to cancel and satisfy the consistency equation

$$\mu \frac{d}{d\mu} \ln(\text{Tr}[\mathbf{S}(b, \mu, \nu) \cdot \mathbf{H}(P_\perp, \mu)]) + \gamma_\mu^{f_a} + \gamma_\mu^{f_b} + \gamma_\mu^{\text{cs}_c} + \gamma_\mu^{\text{cs}_d} + \gamma_\mu^{J_c} + \gamma_\mu^{J_d} = 0. \quad (95)$$

From Eqs. (67), (68), (80), (83), we immediately find at 1-loop,

$$\begin{aligned} \mu \frac{d}{d\mu} \ln(\text{Tr}[\mathbf{S}(b, \mu, \nu) \cdot \mathbf{H}(P_\perp, \mu)]) &= \frac{\text{Tr}[\mathbf{\Gamma}_\mu^{\text{S}\dagger} \cdot \mathbf{S} \cdot \mathbf{H} + \mathbf{S} \cdot \mathbf{\Gamma}_\mu^{\text{S}} \cdot \mathbf{H} + \mathbf{S} \cdot \mathbf{\Gamma}^{\text{H}} \cdot \mathbf{H} + \mathbf{S} \cdot \mathbf{H} \cdot \mathbf{\Gamma}^{\text{H}\dagger}]}{\text{Tr}[\mathbf{S}(b, \mu, \nu) \cdot \mathbf{H}(P_\perp, \mu)]} \\ &= -\frac{\alpha_s}{\pi} \left[ C_a \ln \left( \frac{\nu^2}{x_a^2 S} \right) + C_b \ln \left( \frac{\nu^2}{x_b^2 S} \right) - (C_c + C_d) \ln \left( \frac{P_\perp^2}{\mu_b^2} \right) \right] + 2\gamma_H. \end{aligned} \quad (96)$$

One can then easily check from the  $\mu$ -anomalous dimensions of the other functions given in Eqs. (71), (91), (94) that Eq. (95) is explicitly satisfied at 1-loop.

### D. Resummation formula

Based on the above discussions and RG renormalization group methods in SCET, we could derive all-order resummation results. Explicitly, we calculate the cross section at the NLL accuracy, where we will use the two-loop cusp and one-loop single logarithmic anomalous dimension and the matching coefficients are kept at the leading order. Besides, the color structures inside the hard and soft function will mix with each other under the RG evolution, which was first studied in [65]. In this paper, we will apply the same methods in [92] to solve the RG equations. For the unpolarized cross section, the resummation formula has the form as follows:

$$\begin{aligned} \frac{d\sigma}{dy_c dy_d dP_\perp^2 d^2\vec{q}_\perp} &= \sum_{abcd} \frac{1}{16\pi^2 \hat{s}^2} \frac{1}{N_{\text{init}}} \frac{1}{1 + \delta_{cd}} \frac{1}{2\pi} \int_0^\infty db b J_0(q_\perp b) x_a f_a(x_a, \mu_{b_*}) x_b f_b(x_b, \mu_{b_*}) \\ &\times \exp \left\{ - \int_{\mu_{b_*}}^{\mu_h} \frac{d\mu}{\mu} \left[ \gamma_{\text{cusp}}(\alpha_s) c_H \ln \frac{|\hat{t}|}{\mu^2} + 2\gamma_H(\alpha_s) \right] \right\} \\ &\times \sum_{KK'} \exp \left[ - \int_{\mu_{b_*}}^{\mu_h} \frac{d\mu}{\mu} \gamma_{\text{cusp}}(\alpha_s) (\lambda_K + \lambda_{K'}^*) \right] H_{KK'}(P_\perp, \mu_h) \tilde{S}_{K'K}(b_*, \mu_{b_*}) \\ &\times \exp \left[ - \int_{\mu_{b_*}}^{\mu_j} \frac{d\mu}{\mu} \gamma_\mu^{J_c}(\alpha_s) - \int_{\mu_{b_*}}^{\mu_{cs}} \frac{d\mu}{\mu} \gamma_\mu^{\text{cs}_c}(\alpha_s) \right] U_{\text{NG}}^c(\mu_{cs}, \mu_j) J_c(P_\perp R, \mu_j) S_c^{\text{cs}}(b_*, R, \mu_{cs}) \\ &\times \exp \left[ - \int_{\mu_{b_*}}^{\mu_j} \frac{d\mu}{\mu} \gamma_\mu^{J_d}(\alpha_s) - \int_{\mu_{b_*}}^{\mu_{cs}} \frac{d\mu}{\mu} \gamma_\mu^{\text{cs}_d}(\alpha_s) \right] U_{\text{NG}}^d(\mu_{cs}, \mu_j) J_d(P_\perp R, \mu_j) S_d^{\text{cs}}(b_*, R, \mu_{cs}), \\ &\times \exp \left[ - S_{\text{NP}}^a(b; Q_0, \sqrt{\hat{s}}) - S_{\text{NP}}^b(b; Q_0, \sqrt{\hat{s}}) \right], \end{aligned} \quad (97)$$

where  $\lambda_K$  is the eigenvalue of the matrix  $M_{IJ}$  in the hard anomalous dimension (63) and  $H_{KK'}$  and  $\tilde{S}_{K'K}$  are the hard and soft function in the diagonal basis as defined in [92]. In our numerical calculation instead of using analytical

expressions we apply LAPACK library [100] to obtain their value at each phase-space point. Besides, we have applied the  $b^*$ -prescription to prevent the Landau pole from being reached in the  $b$ -integral. Here we have  $b_*$  defined as

$$b_* = b/\sqrt{1 + b^2/b_{\max}^2}, \quad (98)$$

where  $b_{\max}$  is chosen [101] to be 1.5 GeV<sup>-1</sup>. The nonperturbative Sudakov factor is given as

$$S_{\text{NP}}^{a,b}(b; Q_0, \mu) = g_1^f b^2 + \frac{g_2}{2} \frac{C_{a,b}}{C_F} \ln \frac{\mu}{Q_0} \ln \frac{b}{b_*}, \quad \text{with } g_1^f = 0.106, \quad g_2 = 0.84, \quad Q_0^2 = 2.4 \text{ GeV}^2. \quad (99)$$

In Eq. (97), we also incorporate NGLs resummation effects included by the function  $U_{\text{NG}}^{c,d}$ . In section IV C, we have discussed RG consistence at the one-loop order. While in order to also include NGLs resummation effects at NLL accuracy we also need to consider the extra one-loop single logarithmic anomalous dimension  $\hat{\Gamma}$  from the non-linear evolution parts, and this anomalous dimension is canceled between the jet and collinear-soft function which was verified at the two-loop order [82, 83]. The explicit operator-based derivation of RG consistence including  $\hat{\Gamma}$  can be found in [56, 86, 102]. In the large  $N_c$  limit, the non-linear evolution equation can be solved using the parton shower algorithm [103]. Especially, at the NLL accuracy the evolution is totally determined by the one-loop anomalous dimension  $\hat{\Gamma}$  which is equivalent to the one appearing in the light jet mass distribution at the  $e^+e^-$  collider. Therefore, we can use the same fitting function form given in [81] to capture NGLs resummation contributions after setting proper initial and final evolution scales. In our case these two scales are jet scale  $\mu_j$  and collinear-soft scale  $\mu_{cs}$ . Explicitly, the function is

$$U_{\text{NG}}^k(\mu_{cs}, \mu_j) = \exp \left[ -C_A C_k \frac{\pi^2}{3} u^2 \frac{1 + (au)^2}{1 + (bu)^c} \right], \quad (100)$$

where the superscript  $k = q$  and  $g$  denote the (anti-)quark and gluon jet, respectively, and with  $C_q = C_F$  and  $C_g = C_A$ . The parameters  $a$ ,  $b$  and  $c$  are fitting parameters which are given as  $a = 0.85 C_A$ ,  $b = 0.86 C_A$  and  $c = 1.33$ . The variable  $u = \frac{1}{\beta_0} \log \frac{\alpha_s(\mu_{cs})}{\alpha_s(\mu_j)}$  is the evolution scale measuring the separation of the scales  $\mu_{cs}$  and  $\mu_j$ .

As we have done for the unpolarized cross section, we also derive a similar resummation formula for the spin-dependent cross section

$$\begin{aligned} \frac{d\Delta\sigma(S_\perp)}{dy_c dy_d dP_\perp^2 d^2\vec{q}_\perp} &= \sin(\phi_q - \phi_S) \sum_{abcd} \frac{1}{16\pi^2 \hat{s}^2} \frac{1}{N_{\text{init}}} \frac{1}{1 + \delta_{cd}} \left( -\frac{1}{4\pi} \right) \int_0^\infty db b^2 J_1(q_\perp b) x_a T_{a,F}(x_a, x_a, \mu_{b_*}) x_b f_b(x_b, \mu_{b_*}) \\ &\times \exp \left\{ -\int_{\mu_{b_*}}^{\mu_h} \frac{d\mu}{\mu} \left[ \gamma_{\text{cusp}}(\alpha_s) c_H \ln \frac{|\hat{t}|}{\mu^2} + 2\gamma_H(\alpha_s) \right] \right\} \\ &\times \sum_{KK'} \exp \left[ -\int_{\mu_{b_*}}^{\mu_h} \frac{d\mu}{\mu} \gamma_{\text{cusp}}(\alpha_s) (\lambda_K + \lambda_{K'}^*) \right] H_{KK'}(P_\perp, \mu_h) \tilde{S}_{K'K}(b_*, \mu_{b_*}) \\ &\times \exp \left[ -\int_{\mu_{b_*}}^{\mu_j} \frac{d\mu}{\mu} \gamma_\mu^{J_c}(\alpha_s) - \int_{\mu_{b_*}}^{\mu_{cs}} \frac{d\mu}{\mu} \gamma_\mu^{cs_c}(\alpha_s) \right] U_{\text{NG}}^c(\mu_{cs}, \mu_j) J_c(P_\perp R, \mu_j) S_c^{\text{cs}}(b_*, R, \mu_{cs}) \\ &\times \exp \left[ -\int_{\mu_{b_*}}^{\mu_j} \frac{d\mu}{\mu} \gamma_\mu^{J_d}(\alpha_s) - \int_{\mu_{b_*}}^{\mu_{cs}} \frac{d\mu}{\mu} \gamma_\mu^{cs_d}(\alpha_s) \right] U_{\text{NG}}^d(\mu_{cs}, \mu_j) J_d(P_\perp R, \mu_j) S_d^{\text{cs}}(b_*, R, \mu_{cs}), \\ &\times \exp \left[ -S_{\text{NP}}^s(b; Q_0, \sqrt{\hat{s}}) - S_{\text{NP}}^b(b; Q_0, \sqrt{\hat{s}}) \right], \end{aligned} \quad (101)$$

where at the NLL accuracy we keep the LO matching coefficient in Eq. (15). It involves the parametrization for the Sivvers function, which depends on the collinear Qiu-Sterman function  $T_{q,F}(x_a, x_a, \mu_{b_*})$  and a different non-perturbative Sudakov factor  $S_{\text{NP}}^s$ . The relevant parametrization has been determined from a recent global analysis of the Sivvers asymmetry of SIDIS and Drell-Yan processes [104]. The non-perturbative Sudakov factor is given by

$$S_{\text{NP}}^s(b; Q_0, \mu) = g_1^s b^2 + \frac{g_2}{2} \ln \frac{\mu}{Q_0} \ln \frac{b}{b_*}, \quad \text{with } g_1^s = 0.18. \quad (102)$$

## V. PHENOMENOLOGY

In this section we will present the numerical results using the resummation formula in Eqs. (97) and (101), where intrinsic scales for the hard, jet and collinear-soft function are chosen as

$$\mu_h = \sqrt{\hat{s}}, \quad \mu_j = P_\perp R, \quad \mu_{cs} = \mu_{b_*} R. \quad (103)$$

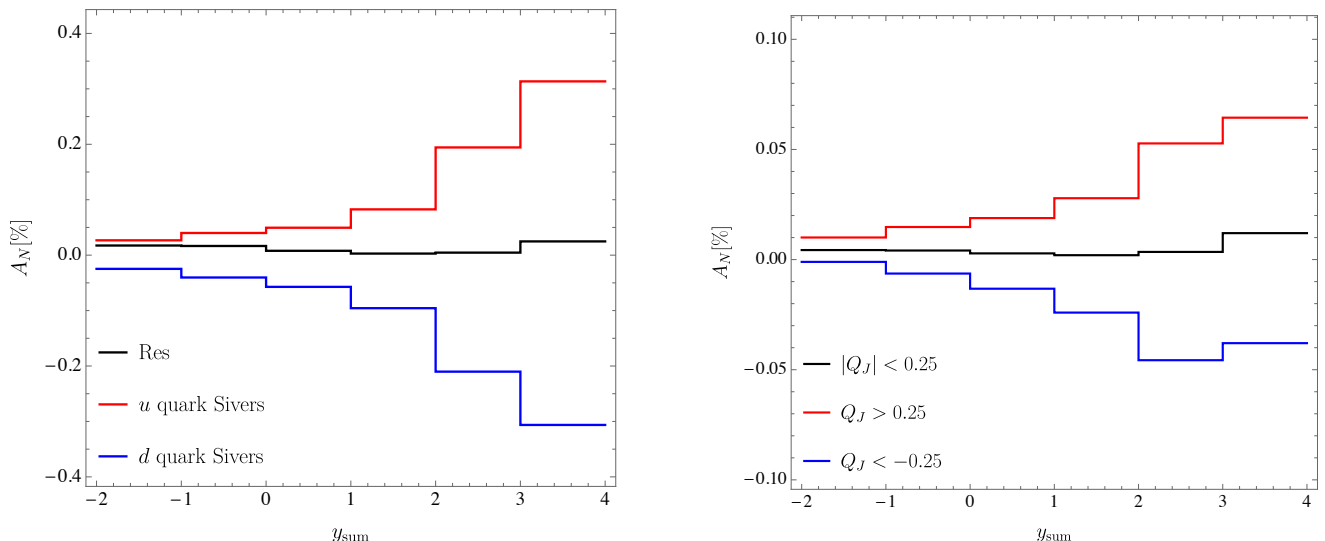


FIG. 5. Theoretical predictions of the Siverts asymmetry for dijet production at the RHIC with  $\sqrt{s} = 200$  GeV. In the left plot red and blue curves are the results from  $u$ - and  $d$ - quark Siverts function, and the black curve includes all the contributions. In the right plot we show the Siverts asymmetry distribution within three different jet charge  $Q_J$  bins.

In the numerical study, we will focus on the Siverts asymmetry for the dijet production at the RHIC with  $\sqrt{s} = 200$  GeV, where the jet events are reconstructed by using anti- $k_T$  algorithm with jet radius  $R = 0.6$ . The transverse momentum  $P_\perp$  and the rapidity  $y_{c,d}$  of jets are

$$P_\perp > 4 \text{ GeV}, \quad -1 < y_{c,d} < 2. \quad (104)$$

For the unpolarized proton we use the HERAPDF20NLO parton distribution functions [105]. Furthermore, the Eq. (9) is derived after neglecting the power corrections from  $\mathcal{O}(q_\perp^2/P_\perp^2)$ . In other words, in the large  $q_\perp$  region, the full results should include corrections from the so-called  $Y$ -term, which can be obtained from perturbative QCD calculations [106]. In this paper we focus on the contribution from back-to-back dijet production. In order to select such kinematics, we require the transverse momentum  $q_\perp$  for the dijet system  $|q_\perp| < q_\perp^{\text{cut}}$ . In the numerical calculations we fix the value of  $q_\perp^{\text{cut}} = 2$  GeV.

As shown in the Fig. 1 the transverse-polarized proton moves on  $+z$ -direction and its spin points to  $+y$ -direction with  $\phi_S = \pi/2$ . The transverse momentum vector  $\vec{q}_\perp$  lies in the  $x - y$  plane, and the Siverts asymmetry is defined as the difference of the events between  $q_{\perp,x} > 0$  and  $q_{\perp,x} < 0$  hemispheres, that is the same as the measurements by STAR collaboration [41]. Explicitly, we have

$$A_N(y_{\text{sum}}) = \frac{\int_0^{q_\perp^{\text{cut}}} dq_\perp \int_0^{2\pi} d\phi_q \int d\mathcal{PS} \frac{d\Delta\sigma}{dq_\perp d\phi_q dy_c dy_d dP_\perp} \left[ \theta(\cos\phi_q) - \theta(-\cos\phi_q) \right]}{\int_0^{q_\perp^{\text{cut}}} dq_\perp \int_0^{2\pi} d\phi_q \int d\mathcal{PS} \frac{d\sigma}{dq_\perp d\phi_q dy_c dy_d dP_\perp}}, \quad (105)$$

with  $\int d\mathcal{PS} = \int dy_c dy_d dP_\perp \delta(y_{\text{sum}} - y_c - y_d)$  represents the transverse momenta and rapidities integral for dijets. In the numerator the  $\phi_q$ -integral with  $\theta(\cos\phi_q)$  and  $\theta(-\cos\phi_q)$  corresponds  $q_{\perp,x} > 0$  and  $q_{\perp,x} < 0$ , respectively.

In the Fig. 5 we show the numerical results of the Siverts asymmetry for dijet processes, where we neglect the charm and bottom jet events. The red and blue curves represent the asymmetry contributed from  $u$ - and  $d$ -quark Siverts function, respectively. As is expected, we find that the asymmetry is enhanced in the large  $y_{\text{sum}}$  region, i.e. the forward scattering region, due to the larger fractional contribution of Siverts function in the valence region. Besides, the contributions from  $u$ - and  $d$ -quark Siverts function are opposite from each other, which causes a huge cancellation of the asymmetry, as shown by the black curves in Fig. 5.

In the calculation, most of the asymmetries come from the partonic scattering process  $qg \rightarrow qg$  where the initial quark comes from the polarized proton. Especially, the more forward jet is associated with the parton from the polarized proton moving in the same direction. Hence, if we can tag parton species initiating the more forward jet, then we can separate  $u$ - and  $d$ -quark Siverts functions and avoid the accidental cancellation as shown in the left plot of Fig. 5.

In order to achieve jet flavor separation mentioned above, one possible method is applying the electric charge information of jets, which has been proposed in [50, 58, 107]. In this paper we will use the standard jet electric charge

definition given in [108, 109]

$$Q_\kappa^i = \sum_h Q_\kappa^h \equiv \sum_{h \in \text{jet}} z_h^\kappa Q_h, \quad (106)$$

where the index  $i$  indicates the parton species initiating the jet and  $z_h$  is the transverse momentum ratio between hadrons and the jet.  $\kappa$  is an input parameter, which is fixed by  $\kappa = 0.3$  in our calculations. As shown in [58], after measuring the jet charge information, the theory formula is slightly modified by replacing the jet function  $J_i(P_\perp R, \mu)$  in Eq. (16) by the charge-tagged jet function  $\mathcal{G}_i(Q_J, P_\perp R, \mu)$  as

$$\frac{d\Delta\sigma}{dQ_J d^2q_\perp} = \int d\mathcal{P}\mathcal{S} T_{a,F} \otimes f_b \otimes \text{Tr}[\mathbf{H} \cdot \mathbf{S}] \otimes S_c^{cs} \otimes S_d^{cs} [\mathcal{G}_c J_d \theta(y_c - y_d) + J_c \mathcal{G}_d \theta(y_d - y_c)], \quad (107)$$

with the normalization as  $\int_{-\infty}^{\infty} dQ_J \mathcal{G}_i(Q_J, P_\perp R, \mu) = J_i(P_\perp R, \mu)$  required by the probability conservation. Here we only replace the more forward jet function with the charge-tagged jet function, which corresponds to the insertion of the step function. We define the jet charge bin fraction as

$$r_i^{\text{bin}} = \frac{\int_{\text{bin}} dQ_J \mathcal{G}_i(Q_J, P_\perp R, \mu)}{J_i(P_\perp R, \mu)}. \quad (108)$$

Then the Siverson asymmetry  $A_N$  in different jet charge bins is given as, in terms of jet charge bin fraction

$$A_N^{\pm,0} = \frac{\sum_{i=u,d,g,\dots} r_i^{\pm,0} \Delta\sigma_i}{\sigma}, \quad (109)$$

where we suppress the phase space integral shown in Eq. (105). The index  $i$  denotes the parton species initiating the more forward jet. Here we use the same jet charge bins defined in [58], where  $+$ ,  $-$  and  $0$  indicate  $Q_J > 0.25$ ,  $Q_J < -0.25$  and  $|Q_J| < 0.25$  bins, separately. Such jet charge bin fraction can be fitted from the unpolarized cross section for back-to-back dijet events at the RHIC. In [50], the authors have shown the preliminary results from the measurements as  $\kappa = 0$ . In the theory calculation, one can use Monte-Carlo event generators such as Pythia8 [110] to estimate these numbers. For the quark jet cases we will use the fractions given in [58], and for the gluon jet we find  $r^+ = 0.36$ ,  $r^- = 0.36$ ,  $r^0 = 0.28$  where the jet charges are defined using  $\pi^\pm$  inside the jet.

In the right plot of Fig. 5 we show the result of  $A_N$  within the different jet charge bins. After selecting the charge of the more forward jet  $Q_J > 0.25$ , the contribution from the  $u$ -quark Siverson function is enhanced compared to the case without the jet charge measurement (the black curve in the left plot). A similar size enhancement from the  $d$ -quark Siverson function is also observed in  $Q_J < -0.25$  charge bin as shown by the blue curve. Besides, we find the Siverson asymmetries from  $Q_J > 0.25$  bins are positive and  $Q_J < -0.25$  bins are negative, which are consistent with the preliminary STAR measurements [50]. In the forward region, the Siverson asymmetry can achieve  $\mathcal{O}(0.1\%)$ , and size of our calculation is also around the same order of the data. Taken together, our calculation suggests that the dijet production at the hadron collider is an important process to extract the information about the Siverson function and deserves further studies on the theoretical framework about the remarks discussed in II C.

## VI. CONCLUSIONS

We study the single spin asymmetries of dijet production in the back-to-back region in transversely polarized proton-proton collisions. In the back-to-back region, the dijet transverse momentum imbalance  $q_\perp$  is much smaller than the transverse momentum  $P_\perp$  of the jets. In this case, the conventional perturbative QCD calculations in the expansion of coupling constant  $\alpha_s$  generate large logarithms in the form of  $\alpha_s^n \ln^m(P_\perp^2/q_\perp^2)$  with  $m \leq 2n - 1$ , which have to be resummed in order to render the convergence of the perturbative computations. We propose a QCD formalism in terms of transverse momentum dependent (TMD) parton distribution functions for dijet production in both unpolarized and polarized proton-proton collisions. Such a formalism allows us to resum the aforementioned large logarithms, and further takes into account the non-universality or process-dependence of the Siverson functions in the case of the transversely polarized scattering. It is well-known that hadronic dijet production in back-to-back region suffers from TMD factorization breaking effects. Thus, to write down the QCD “seemingly factorized” formalism for resumming large logarithms mentioned above, we make a couple of approximations. First of all, we neglect the Glauber mode in the formalism which are known to be the main reason for the TMD factorization breaking. Secondly, we have assumed that the soft gluon radiation that is encoded in the global soft function in our formalism is spin-independent, i.e., they are the same between the unpolarized and polarized scatterings. Since how to exactly deal with the TMD

factorization breaking effects is still an open question, we feel that the proposed formalism in this paper is a reasonable starting point for further investigation.

With such a formalism at hand, we compute the Sivers asymmetry for the dijet production in the kinematic region that is relevant to the proton-proton collisions at the Relativistic Heavy Ion Collider (RHIC), and find that the spin asymmetry is very small due to the cancellation between  $u$ - and  $d$ -quark Sivers functions, which are similar in size but opposite in sign. However, we find that the individual contribution from  $u$ - and  $d$ -quark Sivers functions can lead to an asymmetry of size  $\mathcal{O}(\pm 0.4\%)$  in the forward rapidity region, which seems feasible at the RHIC. Motivated by this, we compute the Sivers asymmetry of dijet production in the positive and negative jet charge bins, i.e., when the jet charge  $Q_J$  for the jet with the larger rapidity of two is in the bins  $Q_J > 0.25$  and  $Q_J < -0.25$ , respectively. By selecting the positive (negative) jet charge bin, we enhance the contribution from  $u$ - ( $d$ -)quark Sivers function and thus enhance the size of the asymmetry. Our calculation shows that Sivers asymmetries in such positive (negative) jet charge bins lead to asymmetries of size  $\mathcal{O}(+0.1\%)$  ( $\mathcal{O}(-0.1\%)$ ), respectively. The sign of such asymmetries seem to be consistent with the preliminary STAR measurements at the RHIC. The size of our calculations is also around the same order of the experimental data. This give us a great hope to further investigate the single spin asymmetries for hadronic dijet production at the RHIC.

### ACKNOWLEDGEMENTS

We thank Huanzhao Liu for useful correspondence on the experimental measurements, thank Maarten Buffing for collaborating during the early stages of this project and thank Zelong Liu for useful discussions. Z.K. and D.Y.S. are supported by the National Science Foundation under Grant No. PHY-1720486 and CAREER award PHY-1945471. K.L. is supported by the National Science Foundation under Grant No. PHY-1316617 and No. PHY-1620628. J.T. is supported by NSF Graduate Research Fellowship Program under Grant No. DGE-1650604. D.Y.S. is also supported by Center for Frontiers in Nuclear Science of Stony Brook University and Brookhaven National Laboratory. This work is supported within the framework of the TMD Topical Collaboration.

*Note added:* While this work was being written up, we noticed a similar work [111] appears on arXiv. The authors investigate process dependent factorization violation from the soft gluon radiation, which is different from our approach. We explicitly calculate the process dependent polarized hard function in the matrix form, which can be used to study the color structure mixing effects under QCD evolution beyond the leading-logarithmic accuracy. Besides, in the numerical calculations we include quark Sivers functions in all the partonic channels. We believe these two studies are complementary with each other.

- 
- [1] D. Boer *et al.*, (2011), arXiv:1108.1713.
  - [2] A. Accardi *et al.*, Eur. Phys. J. A **52**, 268 (2016), arXiv:1212.1701.
  - [3] C. A. Aidala *et al.*, *Probing Nucleons and Nuclei in High Energy Collisions* (WSP, 2020), arXiv:2002.12333.
  - [4] D. W. Sivers, Phys. Rev. D **41**, 83 (1990).
  - [5] D. W. Sivers, Phys. Rev. D **43**, 261 (1991).
  - [6] J. Antille *et al.*, Phys. Lett. B **94**, 523 (1980).
  - [7] E581, E704, D. Adams *et al.*, Phys. Lett. B **261**, 201 (1991).
  - [8] STAR, J. Adams *et al.*, Phys. Rev. Lett. **92**, 171801 (2004), arXiv:hep-ex/0310058.
  - [9] BRAHMS, I. Arsene *et al.*, Phys. Rev. Lett. **101**, 042001 (2008), arXiv:0801.1078.
  - [10] STAR, B. Abelev *et al.*, Phys. Rev. Lett. **101**, 222001 (2008), arXiv:0801.2990.
  - [11] STAR, L. Adamczyk *et al.*, Phys. Rev. D **86**, 051101 (2012), arXiv:1205.6826.
  - [12] PHENIX, A. Adare *et al.*, Phys. Rev. D **90**, 012006 (2014), arXiv:1312.1995.
  - [13] STAR, L. Adamczyk *et al.*, Phys. Rev. D **97**, 032004 (2018), arXiv:1708.07080.
  - [14] G. L. Kane, J. Pumplin, and W. Repko, Phys. Rev. Lett. **41**, 1689 (1978).
  - [15] J.-w. Qiu and G. F. Sterman, Phys. Rev. Lett. **67**, 2264 (1991).
  - [16] C. Kouvaris, J.-W. Qiu, W. Vogelsang, and F. Yuan, Phys. Rev. D **74**, 114013 (2006), arXiv:hep-ph/0609238.
  - [17] Z.-B. Kang, F. Yuan, and J. Zhou, Phys. Lett. B **691**, 243 (2010), arXiv:1002.0399.
  - [18] Z.-B. Kang, J.-W. Qiu, W. Vogelsang, and F. Yuan, Phys. Rev. D **83**, 094001 (2011), arXiv:1103.1591.
  - [19] A. Metz and D. Pitonyak, Phys. Lett. B **723**, 365 (2013), arXiv:1212.5037, [Erratum: Phys.Lett.B 762, 549–549 (2016)].
  - [20] L. Gamberg, Z.-B. Kang, and A. Prokudin, Phys. Rev. Lett. **110**, 232301 (2013), arXiv:1302.3218.
  - [21] K. Kanazawa, Y. Koike, A. Metz, and D. Pitonyak, Phys. Rev. D **89**, 111501 (2014), arXiv:1404.1033.
  - [22] L. Gamberg, Z.-B. Kang, D. Pitonyak, and A. Prokudin, Phys. Lett. B **770**, 242 (2017), arXiv:1701.09170.
  - [23] J.-w. Qiu and G. F. Sterman, Nucl. Phys. B **378**, 52 (1992).
  - [24] K. Kanazawa and Y. Koike, Phys. Rev. D **82**, 034009 (2010), arXiv:1005.1468.

- [25] J. Cammarota *et al.*, (2020), arXiv:2002.08384.
- [26] HERMES, A. Airapetian *et al.*, Phys. Rev. Lett. **103**, 152002 (2009), arXiv:0906.3918.
- [27] HERMES, A. Airapetian *et al.*, (2020), arXiv:2007.07755.
- [28] COMPASS, C. Adolph *et al.*, Phys. Lett. **B717**, 383 (2012), arXiv:1205.5122.
- [29] COMPASS, C. Adolph *et al.*, Phys. Lett. **B770**, 138 (2017), arXiv:1609.07374.
- [30] Jefferson Lab Hall A, X. Qian *et al.*, Phys. Rev. Lett. **107**, 072003 (2011), arXiv:1106.0363.
- [31] A. Bacchetta *et al.*, JHEP **02**, 093 (2007), arXiv:hep-ph/0611265.
- [32] S. J. Brodsky, D. S. Hwang, and I. Schmidt, Nucl. Phys. B **642**, 344 (2002), arXiv:hep-ph/0206259.
- [33] J. C. Collins, Phys. Lett. B **536**, 43 (2002), arXiv:hep-ph/0204004.
- [34] D. Boer, P. Mulders, and F. Pijlman, Nucl. Phys. B **667**, 201 (2003), arXiv:hep-ph/0303034.
- [35] COMPASS, M. Aghasyan *et al.*, Phys. Rev. Lett. **119**, 112002 (2017), arXiv:1704.00488.
- [36] STAR, L. Adamczyk *et al.*, Phys. Rev. Lett. **116**, 132301 (2016), arXiv:1511.06003.
- [37] Z.-B. Kang and J.-W. Qiu, Phys. Rev. Lett. **103**, 172001 (2009), arXiv:0903.3629.
- [38] M. Anselmino, M. Boglione, U. D'Alesio, F. Murgia, and A. Prokudin, JHEP **04**, 046 (2017), arXiv:1612.06413.
- [39] E.-C. Aschenauer *et al.*, (2016), arXiv:1602.03922.
- [40] AnDY, L. Bland *et al.*, Phys. Lett. B **750**, 660 (2015), arXiv:1304.1454.
- [41] STAR, B. Abelev *et al.*, Phys. Rev. Lett. **99**, 142003 (2007), arXiv:0705.4629.
- [42] D. Boer and W. Vogelsang, Phys. Rev. D **69**, 094025 (2004), arXiv:hep-ph/0312320.
- [43] C. Bomhof, P. Mulders, W. Vogelsang, and F. Yuan, Phys. Rev. D **75**, 074019 (2007), arXiv:hep-ph/0701277.
- [44] W. Vogelsang and F. Yuan, Phys. Rev. D **76**, 094013 (2007), arXiv:0708.4398.
- [45] J.-W. Qiu, W. Vogelsang, and F. Yuan, Phys. Lett. B **650**, 373 (2007), arXiv:0704.1153.
- [46] M. G. Echevarria, A. Idilbi, Z.-B. Kang, and I. Vitev, Phys. Rev. **D89**, 074013 (2014), arXiv:1401.5078.
- [47] A. Bacchetta, F. Delcarro, C. Pisano, and M. Radici, (2020), arXiv:2004.14278.
- [48] J. Collins and J.-W. Qiu, Phys. Rev. D **75**, 114014 (2007), arXiv:0705.2141.
- [49] T. C. Rogers and P. J. Mulders, Phys. Rev. D **81**, 094006 (2010), arXiv:1001.2977.
- [50] H. Liu, *Talk given at RIKEN BNL Workshop Jet Observables at the Electron-Ion Collider*, 2020.
- [51] PHENIX, A. Adare *et al.*, Phys. Rev. D **95**, 072002 (2017), arXiv:1609.04769.
- [52] PHENIX, C. Aidala *et al.*, Phys. Rev. D **98**, 072004 (2018), arXiv:1805.02450.
- [53] P. Sun, C. P. Yuan, and F. Yuan, Phys. Rev. Lett. **113**, 232001 (2014), arXiv:1405.1105.
- [54] P. Sun, C. P. Yuan, and F. Yuan, Phys. Rev. **D92**, 094007 (2015), arXiv:1506.06170.
- [55] M. G. A. Buffing, Z.-B. Kang, K. Lee, and X. Liu, (2018), arXiv:1812.07549.
- [56] Y.-T. Chien, D. Y. Shao, and B. Wu, JHEP **11**, 025 (2019), arXiv:1905.01335.
- [57] Y.-T. Chien *et al.*, (2020), arXiv:2005.12279.
- [58] Z.-B. Kang, X. Liu, S. Mantry, and D. Y. Shao, (2020), arXiv:2008.00655.
- [59] M. Cacciari, G. P. Salam, and G. Soyez, Eur. Phys. J. C **72**, 1896 (2012), arXiv:1111.6097.
- [60] C. W. Bauer, S. Fleming, and M. E. Luke, Phys. Rev. D **63**, 014006 (2000), arXiv:hep-ph/0005275.
- [61] C. W. Bauer, S. Fleming, D. Pirjol, and I. W. Stewart, Phys. Rev. **D63**, 114020 (2001), arXiv:hep-ph/0011336.
- [62] C. W. Bauer and I. W. Stewart, Phys. Lett. **B516**, 134 (2001), arXiv:hep-ph/0107001.
- [63] C. W. Bauer, D. Pirjol, and I. W. Stewart, Phys. Rev. **D65**, 054022 (2002), arXiv:hep-ph/0109045.
- [64] C. W. Bauer, S. Fleming, D. Pirjol, I. Z. Rothstein, and I. W. Stewart, Phys. Rev. **D66**, 014017 (2002), arXiv:hep-ph/0202088.
- [65] N. Kidonakis, G. Oderda, and G. F. Sterman, Nucl. Phys. B **531**, 365 (1998), arXiv:hep-ph/9803241.
- [66] J.-y. Chiu, A. Jain, D. Neill, and I. Z. Rothstein, Phys. Rev. Lett. **108**, 151601 (2012), arXiv:1104.0881.
- [67] J.-Y. Chiu, A. Jain, D. Neill, and I. Z. Rothstein, JHEP **05**, 084 (2012), arXiv:1202.0814.
- [68] J. Collins, Camb. Monogr. Part. Phys. Nucl. Phys. Cosmol. **32**, 1 (2011).
- [69] A. Bacchetta, U. D'Alesio, M. Diehl, and C. Miller, Phys. Rev. D **70**, 117504 (2004), arXiv:hep-ph/0410050.
- [70] Z.-B. Kang, B.-W. Xiao, and F. Yuan, Phys. Rev. Lett. **107**, 152002 (2011), arXiv:1106.0266.
- [71] P. Sun and F. Yuan, Phys. Rev. D **88**, 114012 (2013), arXiv:1308.5003.
- [72] L.-Y. Dai, Z.-B. Kang, A. Prokudin, and I. Vitev, Phys. Rev. D **92**, 114024 (2015), arXiv:1409.5851.
- [73] I. Scimemi, A. Tarasov, and A. Vladimirov, JHEP **05**, 125 (2019), arXiv:1901.04519.
- [74] V. Moos and A. Vladimirov, (2020), arXiv:2008.01744.
- [75] A. Bacchetta, C. Bomhof, P. Mulders, and F. Pijlman, Phys. Rev. D **72**, 034030 (2005), arXiv:hep-ph/0505268.
- [76] C. Bomhof, P. Mulders, and F. Pijlman, Eur. Phys. J. C **47**, 147 (2006), arXiv:hep-ph/0601171.
- [77] J.-W. Qiu, W. Vogelsang, and F. Yuan, Phys. Rev. D **76**, 074029 (2007), arXiv:0706.1196.
- [78] S. Catani, D. de Florian, and G. Rodrigo, JHEP **07**, 026 (2012), arXiv:1112.4405.
- [79] J. R. Forshaw, M. H. Seymour, and A. Siodmok, JHEP **11**, 066 (2012), arXiv:1206.6363.
- [80] I. Z. Rothstein and I. W. Stewart, JHEP **08**, 025 (2016), arXiv:1601.04695.
- [81] M. Dasgupta and G. P. Salam, Phys. Lett. **B512**, 323 (2001), arXiv:hep-ph/0104277.
- [82] T. Becher, M. Neubert, L. Rothen, and D. Y. Shao, Phys. Rev. Lett. **116**, 192001 (2016), arXiv:1508.06645.
- [83] T. Becher, M. Neubert, L. Rothen, and D. Y. Shao, JHEP **11**, 019 (2016), arXiv:1605.02737, [Erratum: JHEP05,154(2017)].
- [84] G. F. Sterman, Acta Phys. Polon. **B36**, 389 (2005), arXiv:hep-ph/0410014.
- [85] T. Becher, R. Rahn, and D. Y. Shao, JHEP **10**, 030 (2017), arXiv:1708.04516.
- [86] Z.-B. Kang, D. Y. Shao, and F. Zhao, (2020), arXiv:2007.14425.

- [87] M. Dasgupta and G. P. Salam, JHEP **03**, 017 (2002), arXiv:hep-ph/0203009.
- [88] M. Balsiger, T. Becher, and D. Y. Shao, JHEP **04**, 020 (2019), arXiv:1901.09038.
- [89] D. Neill, JHEP **02**, 114 (2019), arXiv:1808.04897.
- [90] A. Banfi, G. Marchesini, and G. Smye, JHEP **08**, 006 (2002), arXiv:hep-ph/0206076.
- [91] Y. Hatta, E. Iancu, A. H. Mueller, and D. N. Triantafyllopoulos, JHEP **02**, 075 (2018), arXiv:1710.06722.
- [92] R. Kelley and M. D. Schwartz, Phys. Rev. D **83**, 045022 (2011), arXiv:1008.2759.
- [93] Z. L. Liu, C. S. Li, J. Wang, and Y. Wang, JHEP **04**, 005 (2015), arXiv:1412.1337.
- [94] I. Moulst, I. W. Stewart, F. J. Tackmann, and W. J. Waalewijn, Phys. Rev. D **93**, 094003 (2016), arXiv:1508.02397.
- [95] T. Becher and M. Neubert, JHEP **06**, 081 (2009), arXiv:0903.1126, [Erratum: JHEP **11**, 024 (2013)].
- [96] G. F. Sterman and M. E. Tejeda-Yeomans, Phys. Lett. B **552**, 48 (2003), arXiv:hep-ph/0210130.
- [97] A. Hornig, D. Kang, Y. Makris, and T. Mehen, JHEP **12**, 043 (2017), arXiv:1708.08467.
- [98] S. D. Ellis, C. K. Vermilion, J. R. Walsh, A. Hornig, and C. Lee, JHEP **11**, 101 (2010), arXiv:1001.0014.
- [99] X. Liu and F. Petriello, Phys. Rev. D **87**, 014018 (2013), arXiv:1210.1906.
- [100] E. Anderson *et al.*, *LAPACK Users' Guide*, Third ed. (Society for Industrial and Applied Mathematics, Philadelphia, PA, 1999).
- [101] Z.-B. Kang, A. Prokudin, P. Sun, and F. Yuan, Phys. Rev. **D93**, 014009 (2016), arXiv:1505.05589.
- [102] T. Becher, B. D. Pecjak, and D. Y. Shao, JHEP **12**, 018 (2016), arXiv:1610.01608.
- [103] M. Balsiger, T. Becher, and D. Y. Shao, JHEP **08**, 104 (2018), arXiv:1803.07045.
- [104] M. G. Echevarria, Z.-B. Kang, and J. Terry, *in preparation*, 2020.
- [105] H1, ZEUS, H. Abramowicz *et al.*, Eur. Phys. J. C **75**, 580 (2015), arXiv:1506.06042.
- [106] J. Currie *et al.*, Phys. Rev. Lett. **119**, 152001 (2017), arXiv:1705.10271.
- [107] E.-C. Aschenauer *et al.*, (2015), arXiv:1501.01220.
- [108] D. Krohn, M. D. Schwartz, T. Lin, and W. J. Waalewijn, Phys. Rev. Lett. **110**, 212001 (2013), arXiv:1209.2421.
- [109] W. J. Waalewijn, Phys. Rev. D **86**, 094030 (2012), arXiv:1209.3019.
- [110] T. Sjostrand, S. Mrenna, and P. Z. Skands, Comput. Phys. Commun. **178**, 852 (2008), arXiv:0710.3820.
- [111] X. Liu, F. Ringer, W. Vogelsang, and F. Yuan, (2020), arXiv:2008.03666.